

# Etching of diamond

## **1. Introduction**

The extreme properties of diamond make it an extremely versatile and useful material. However, its hardness and chemical inertness, although useful in many applications, are also problematic due to the resulting difficulty in smoothing and shaping the diamond.

### **1.2 Chemical Etchants**

#### **1.2.1 Polishing**

Throughout its use as a cutting tool coating, it has been observed that certain materials damage the diamond surface more than others. This has led to the understanding that it is superior carbon solvents that result in higher wear of the diamond surface [1]. Therefore, many chemical etching processes have been proposed and developed in order to achieve maximisation of the effectiveness of polishing the diamond surface.

The shaping of bulk diamond crystals has proved easier than for CVD diamond films because of the disorganised orientations of the crystal surface in CVD diamond films [2]. Thermochemical polishing is one of the earlier techniques developed to overcome this difficulty and involves the polishing of CVD diamond by sliding a hot metal plate across the surface. The metal used can be altered along with several other variables in order to achieve different polishing times and qualities; the slide speed of the plate over the diamond surface, the pressure applied, the atmosphere and the temperature all have an effect on the polishing outcome.

Applying a large polishing pressure is shown to be unnecessary, as there is only gradual increase in polished area for pressures above approximately 20 kPa [3]. The pressures used in this process are generally lower than for polishing of many other materials, however this is explained by the mechanism of diamond polishing in this way. The applied pressure only aids polishing by closing the gap between the diamond surface and the polishing plate, whereas the actual polishing occurs via diffusion of graphitized carbon into the polishing plate [2,3]. Figure 1 shows how the area of graphitisation is larger than the point of contact, however diffusion of carbon into the metal plate occurs only from the point of contact.

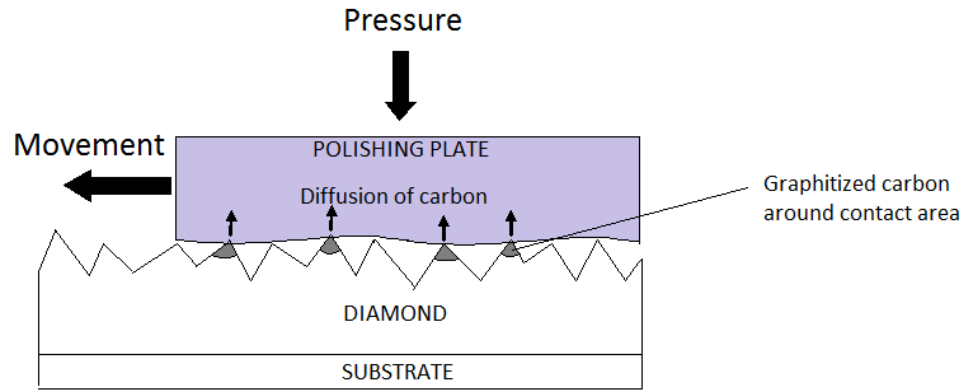


Figure 1. The metal plate polishing of diamond. Diffusion of graphitized carbon into the plate occurs only at the point of contact.

As previously mentioned the polishing of the diamond surface is reliant on the diffusion of carbon into the metal. Therefore varying the material used for the polishing plate alters the efficiency of polishing according to the diffusion coefficient of carbon atoms for the metal. Pure iron has a high diffusion coefficient for carbon, and therefore is commonly used in this process. A nickel polishing plate gives reasonable polishing, however the polished area is not as large as for the iron equivalent, and molybdenum which is known to react with carbon does not achieve any polishing of the surface [3].

The atmosphere during polishing has a significant effect on the polishing rate and the polished surface quality. The order of polishing rates increases in the following order [3]:

$N_2 < He < Ar \ll H_2 \ll \text{vacuum}$ .

Nitrogen results in the slowest polishing rate and it is suggested that this is due to the absorption of nitrogen molecules onto the metal plate surface and thus hindering the diffusion of carbon into the metal [2]. Hydrogen gives a significantly higher polishing rate than the noble gases. This is attributed to a chemical reaction taking place simultaneously with polishing: carbon which has diffused into the metal plate reacts with hydrogen gas in the presence of iron or nickel to give a hydrocarbon [2]. In reacting with diffused carbon, the concentration of carbon in the metal is reduced allowing further diffusion of carbon from the diamond surface and therefore aiding polishing. Reaction with hydrogen at the diamond surface to produce methane could reasonably be assumed to aid polishing; however, the presence of methane after attempted polishing with molybdenum invalidates this theory because as previously stated, no polishing occurs when a molybdenum polishing plate is used [3].

The polishing rate in a vacuum is about twice as fast as in a hydrogen atmosphere. The lower gas density in a vacuum allows the diamond surface and polishing plate to contact more closely, and hence increase the diffusion of carbon into the plate. However, despite this giving the highest polishing rate, the resultant surface is of inferior quality compared to surfaces polished in hydrogen. Oxygen remaining in the system after the vacuum has been established is able to etch the surface and cause hollow pits. A relatively smooth diamond surface is achieved by first polishing under vacuum, and subsequently polishing under a hydrogen atmosphere (figure 2).

Temperature has a large influence on the polishing outcome. The lower limit of temperature for polishing to occur is roughly 700 °C, and the polishing rate increases with increased temperature [3]. However, the polished surface roughness also increases with temperature, and when polishing under vacuum the density of etch pits in the surface also increases with temperature. Finally, the sliding

speed has a relatively small effect on the polishing rate, however a faster sliding speed does aid polishing because the contact between the diamond and the plate is increased [3].

Therefore, considering all variables and the effects they have on polishing, the optimal means of achieving a highly polished surface in a reasonable time is using an iron plate to polish first at high temperature under vacuum, and subsequently at low temperature in hydrogen [3].

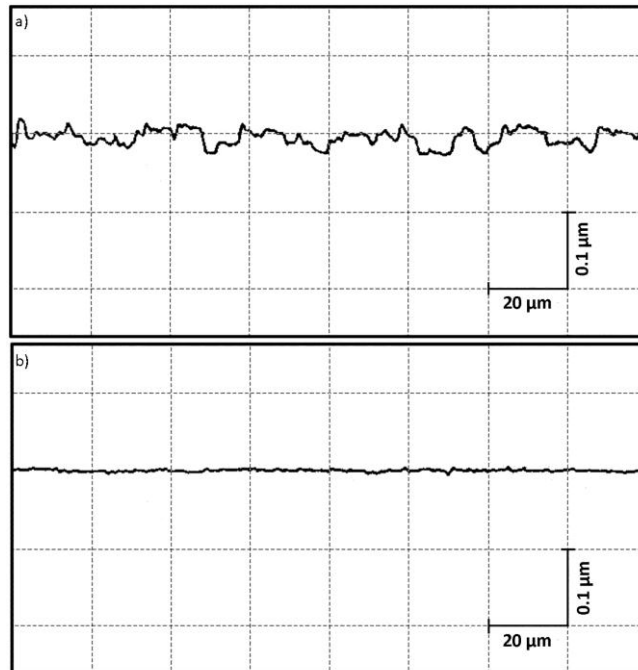


Figure 2 [3] Roughness profiles of CVD diamond surface after hot iron metal plate polishing; a) under vacuum, and b) polishing under vacuum followed by polishing under hydrogen.

In terms of polishing diamond on a commercial scale, from a cost-benefit perspective thermochemical polishing is inefficient. The high temperatures and pressures involved, alongside the requirements on atmosphere mean that the process is expensive, and the quality of the resultant polished surface is not good enough to justify this expense. Also, when repeating the procedure many times for multiple polished diamond films, the conditions result in the deterioration of the metal plate due to softening at high temperature. This results not only in poor polishing rate, but also in small amounts of the metal being transferred on to the diamond surface hindering polishing in that area and reducing the polishing quality [2].

### 1.2.2 Tribochemical Polishing (TCP)

A more recent technique, tribochemical polishing (TCP), seeks to overcome these problems by polishing with a fast rotating metal plate pressed against the metal surface. The polishing is achieved because of the thermochemical reaction that results from friction between the plate and diamond surface. This method is considered to have potential for large scale use; having eliminated the requirement for expensive heating equipment as well as avoiding damage to the polishing plate, efficient and cost effective polishing may be achieved.

The success of TCP is dependent on the selection of the correct metals to make up the polishing plate. Many hypotheses have been explored to determine the reason for certain metals to wear more quickly than others when polishing diamond. Though certain of the best performing plates have similar melting points, crystal structures and material hardness properties, it seems that the property which

best correlates to plate wear is the number of unpaired d electrons of the metal [4]. It has been proposed that the presence of unpaired d electrons means the metal can chemically bond with the carbon on the diamond surface, and this aids polishing by lowering the activation energy for the conversion of diamond to graphite [1]. The graphite is then removed through a mixture of mechanical polishing, oxidation and diffusion into the polishing plate, in the same way as thermochemical polishing.

As well as the unpaired d electron requirement, it is favourable to have bond lengths between the metal atoms such that it can be orientated in such a way as to form vertical bonds with adjacent carbon atoms on the diamond surface. This enhances the conversion of diamond to graphite because the metals effect on the diamond is concentrated on one site. The distances between adjacent carbon atoms in diamond and graphite are shown in figure 3. In the process of conversion from diamond to graphite, the distance between the carbon atoms that the metal bonds to is seen to reduce from 2.51 Å to 2.46 Å. Therefore, a metal with atoms on the same face being roughly 2.51 Å apart will help to reduce the activation energy of conversion from the diamond to graphite structure [Yuan].

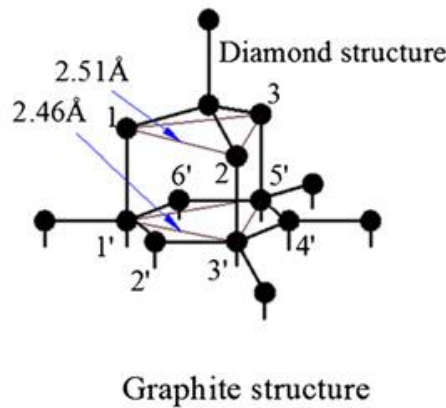


Figure 3 [1]. The lengths between carbon atoms with the correct alignment to form adjacent bonds with the metal structure; shown for both the diamond and graphite forms.

Considering these constraints, a metal or alloy can be chosen for the TCP plate. However, the chosen material must also have high temperature stability in order to avoid degradation of the plate and the poor polishing quality that ensues. Therefore, alternative materials to iron, nickel and stainless steel are currently being sought for the purposes of effective TCP. To date, one of the most effective of these is an FeNiCr alloy [1]. This alloy has been shown to achieve polishing rates of over  $3.5 \mu\text{m min}^{-1}$  and a consequent diamond surface roughness of below  $0.4 \mu\text{m}$  [1]. However, in comparison with other available methods, this polishing rate is relatively slow and hence reduces the wide scale application of TCP to that of a finishing technique [5].

Low temperature techniques for the thinning, etching and polishing of diamond are particularly desirable not only because of the increased cost effectiveness; but also because when manufacturing diamond for semiconductor applications, excessive temperatures can cause damage to dopants within the component [6].

### 1.2.3 Rare-Earth Metal Polishing

Another early technique for the polishing of the diamond surface used molten rare-earth metals known to have a high solubility for carbon. Metals such as lanthanum and cerium have been shown to dissolve a higher percentage of carbon than iron and manganese [7]. An advantage of using a molten

metal is the increase in the diffusion of carbon because of the liquid phase of the etchant [7]. However, this again involves high temperatures (above the melting point of the metal). In order to reduce the required temperature, a procedure was developed whereby the rare-earth metals are combined with other metals to create an alloy of eutectic composition. This allowed the removal of surface diamond at temperatures well below the melting point of the pure rare-earth metal [6]. While this technique had the advantage of being able to process many diamond films simultaneously, the etching times are in the order of days, hence inhibiting the practical application.

## **1.3 Physical Bombardment**

Many physical bombardment techniques exist for the polishing, etching and shaping of the diamond thin film surface. Reactive ion etching (RIE), plasmas and concentrated ion beams are all widely used for this purpose, and each of these methods has many variables that may be altered to achieve different end results.

### **1.3.1 Reactive Ion Etching (RIE)**

RIE employs a plasma for the creation of the ion species, and these etch the diamond surface through a combination of physical sputtering and chemical reaction processes, the ratio of which is determined by the ionic species and radicals present. The presence of these ions allows the use of substrate bias to establish anisotropic etching, something which is essential for more accurate control over creation of patterns and structures in diamond films [8].

One of the advantages of RIE is the large choice of reactants that may be used in the process. Different reactants used for etching result in different surface morphologies, allowing the desired process to be enhanced through selection of the optimum reactant mixture. However, direct quantitative comparison between different reactant systems in RIE is limited by the varying techniques and conditions used [9]. The plasma used as a source of reactive ions, the gaseous atmosphere and the substrate bias are all variable, and the effect of voltage bias can be dependent on the ions present [8].

RIE of CVD diamond films in microwave plasma with varied reactants and voltage bias has been investigated [8]. The introduction of a positive bias to the substrate when etching in hydrogen has no effect on the etch rate, however when a negative substrate bias is applied, the etch rate increases significantly; under negative substrate bias  $H^+$  ions present in the plasma are accelerated towards the diamond film and contribute to the etching whereas the low volume density of  $H^-$  ions means that positive bias has little effect. By increasing the kinetic energy of the  $H^+$  ions, more physical defect sites are produced on the surface meaning the chemical etching pathway by hydrogen atoms is increased. Similar results for bias assisted etching are seen on addition of argon to the hydrogen plasma, however the etch rate is slightly higher in general.

Conversely, when oxygen is added in quantities as small as 2.5%, the effect of voltage bias is reversed; increasing negative substrate bias gives only a small increase in etch rate, whereas positive bias increases the etch rate considerably. The small increase as a result of negative bias is due to the increased concentration of positive hydrogen ions as a result of oxygen's electronegativity. On addition of oxygen, both  $O^-$  and  $OH^-$  ions are formed and hence the ion flux density at the diamond surface under positive bias is increased significantly. In addition, these ions are heavier than the

positive  $H^+$  ions, and hence have higher kinetic energy which also contributes to the increased etch rate.

As well as etch rate, the diamond surface quality after etching is also affected by the varied conditions. Increasing the negative bias in a hydrogen plasma leads to an increased amount of graphitic carbon on the diamond surface after etching. This is a result of increased etching via the physical pathway resulting in higher conversion rates of diamond to graphite. The graphitic carbon is removed from the diamond surface through chemical etching by hydrogen, however when the conversion rate is higher than the rate of graphite removal, an equilibrium layer of graphitic carbon remains. This effect is even greater for H/Ar plasmas, because of the even higher proportion of physical bombardment. In H/O<sub>2</sub> plasmas, despite an increase in ion concentration, less graphitic build up is seen because the graphite removal is accomplished more efficiently through oxygen-carbon and hydroxyl-carbon pathways [8].

In order for RIE to be useful in terms of diamond etching, the result must be reproducible, the process must be efficient and the resulting diamond surface must be of reasonable quality. In light of the above, hydrogen plasma etching does not have many practical applications in terms of etching diamond because the etching rate is slower than for many alternative systems [10]. Argon plasmas have the significant advantage of improving the surface flatness of diamond films through etching [11] and also have reasonable etch rates that can be improved by increasing the pressure of the argon gas [12]. Conversely, increased pressure in the reaction chamber of a CF<sub>4</sub> plasma system results in a decrease in etch rate. This is attributed to the increase in reactive CF<sub>n</sub><sup>+</sup> ion species at lower pressures [11].

It has been shown that there is a correlation between the etching rates of a gas plasma system with the reaction rates of formation of the carbon-gas products [10]. CO and CO<sub>2</sub> have lower enthalpy of formation values than CH<sub>4</sub>, and it therefore is proposed that this is a contributing factor to the higher diamond etching rates of oxygen compared to hydrogen plasmas [10].

When etching under substrate bias, electric field concentration can build at grain boundaries on the CVD diamond surface. This can lead to unfavourable results: ion bombardment is concentrated at grain boundaries, and this can lead to the formation of hillocks on the diamond surface resulting in minimal smoothing of the diamond surface under etching [8]. The use of a protecting SiO<sub>2</sub> bilayer can overcome this problem and result in a higher level of smoothing of the diamond surface [13].

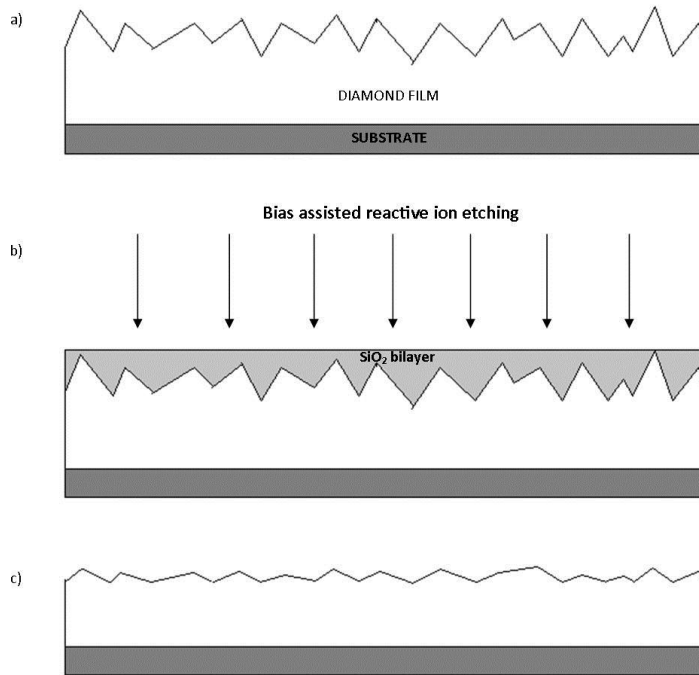


Figure 4. Etching of CVD diamond film using a silicon dioxide bilayer; a) the original diamond surface, b) the SiO<sub>2</sub> coated diamond film prior to etching and c) the resultant diamond film with reduced surface roughness.

Silicon dioxide is a suitable material for this purpose because it is etched at a similar rate to diamond, and can be uniformly deposited onto the diamond surface with relative ease. By depositing a layer of SiO<sub>2</sub> approximately 1.5  $\mu\text{m}$  thick, the diamond peaks are covered and the surface roughness is reduced (figure 4 b). Etching can then be carried out without preferential attack at diamond grain boundaries resulting in an overall smoothing of the diamond surface (figure 4 c). Owing to the slight etching rate differences between diamond and silicon dioxide, a precise etchant gas mixture must be used to ensure both materials are etched at equal rates. A mixture of SF<sub>6</sub> (approximately 10%) with O<sub>2</sub> has been found to etch the bilayer consistently, allowing removal of diamond peaks with almost no reduction in the diamond film thickness[13]. However, the extent of etching must be carefully controlled in order to remove the entire SiO<sub>2</sub> layer without continuing past this point which would result in direct etching of the diamond surface and hence an increase in the surface roughness.

A problem arises from physical sputtering etching when it is coupled with a hard mask lithographic technique for patterned etching. High energy ions employed in physical sputtering have poor selectivity between the diamond surface and typical hard mask materials such as silicon dioxide and aluminium [14]. In order to overcome this problem, an oxygen inductively coupled plasma (ICP) can be used to obtain a smooth etched diamond surface with good selectivity of diamond with respect to mask materials. In order to achieve this, low pressure and low ion potential conditions must be employed. Very high frequency (VHF) plasmas allow plasma stability under these conditions, providing a magnetic guiding field is used to maintain plasma density under low pressure [15].

Oxygen plasmas contain both O<sup>+</sup> and O<sub>2</sub><sup>+</sup> ions, the ratio of which can be manipulated through control of driving frequency, pressure and magnetic field strength[15]. Altering the flux ratio of these ions affects the surface morphology that results from etching, and this is attributed to the different ways in which the respective ions etch the surface. An O<sub>2</sub><sup>+</sup>-rich plasma results in convex protrusions on the etched surface, with initial surface grooves no longer visible (figure 5 a), indicating that a physical reaction is responsible for the etching process. On the contrary, with a high O<sup>+</sup> flux ratio the initial surface grooves remain, and many concave etch pits are present in the etched surface (figure 5 b). This result is comparable to RIE with a High Frequency ICP, and indicates that etching is achieved through a chemical reaction.

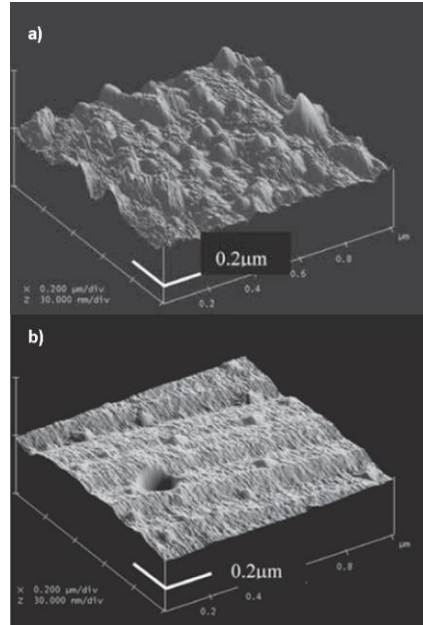


Figure 5 [15]. Oxygen plasma etching of diamond under different molecular ion : atomic ion flux ratios;  
 a)  $O^+/O_2^+ = 16\%$  and b)  $O^+/O_2^+ = 400\%$ .

In order to achieve a smoothed etched diamond surface, a more balanced ratio of atomic and molecular oxygen ions must be used. Experimental evidence shows that an  $O^+/O_2^+$  ratio of 69% is suitable for creation of a smooth diamond surface, whereby etching is achieved through a mixture of both reaction pathways [15]. This technique therefore enables a greater choice of hard masks for lithographic pattern etching, as the need for high energy ions or reactive etchant gases such as  $CF_4$  which have poor selectivity between diamond and mask materials has been avoided.

Hydrogen plasmas have also been shown to successfully etch CVD diamond, however the etch rate can be improved. Addition of  $CH_4$  to hydrogen plasma even in quantities as small as 1.5% enhances the etch rate significantly. This is due to the higher mean energy of the methylic ions with respect to  $H^+$  ions, and results in the methane being dominant in the etching process despite being present in far less quantity than hydrogen [16].

### 1.3.2 Ion Beam Assisted Etching (IBAE)

An alternative method to RIE which has potential to have greater selectivity between diamond and hard masks utilises a reactive gas and an ion beam fired at the diamond surface. A typical ion beam assisted etching (IBAE) setup is shown in figure 6. The  $NO_2$  gas is adsorbed onto the diamond surface and under bombardment from the ion beam, desorption can occur coincident with diamond carbon removal. The ion beam also aids removal through physical sputtering of the diamond surface, and the ratio of these processes is determined by the ions used and their energies, flux density, temperature, pressure and gaseous atmosphere employed. The liquid nitrogen trap is used simply to isolate the reactive gas from the ion source.

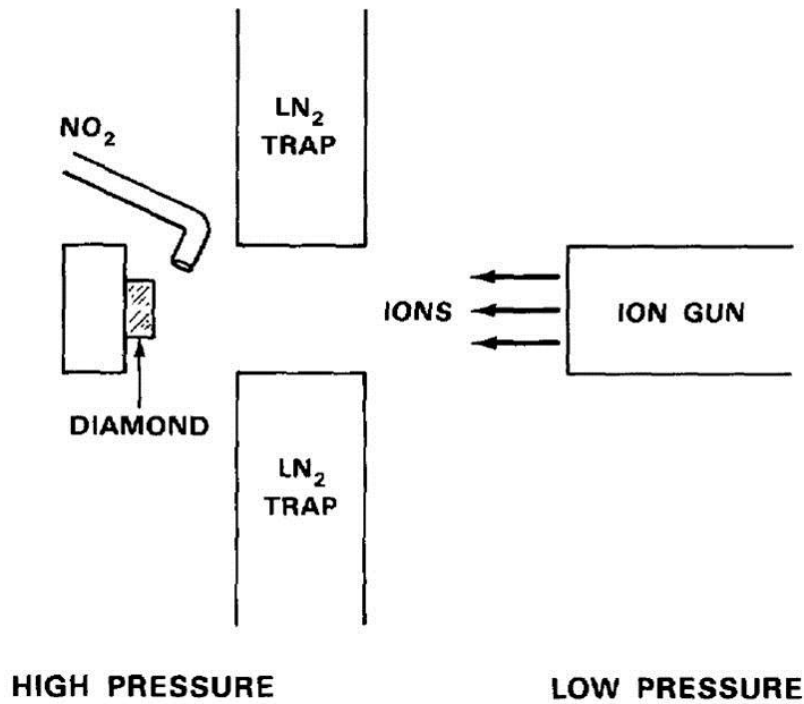


Figure 6 [17] Schematic drawing of an ion beam assisted etching setup.

The use of  $\text{NO}_2$  for the reactive gas has been shown to achieve good etching rates and have advantages over using  $\text{O}_2$ ; the  $\text{NO}_2$  is collected more efficiently by the liquid nitrogen trap, and the ratio of etching rates  $\text{O}_2/\text{NO}_2$  is approximately one third so  $\text{NO}_2$  is favourable as a reactive gas [17]. For pure argon,  $\text{Ar}/\text{O}_2$  and  $\text{Ar}/\text{CF}_4$  gas environments, it is found that the greatest etch rate is achieved with an  $\text{O}_2$  :  $\text{Ar}$  ratio of roughly 1 : 1.5 and that even high proportions of  $\text{CF}_4$  in the argon gas have a very limited effect on etch rate [9], the etch rates for these systems are not as high as for the  $\text{NO}_2$  system used by Efremow *et. al.*[17].

One of the advantages of IBAE over RIE is the ease with which the incident angle can be manipulated. This allows the improvement of surface flatness of the diamond film through removal of features that are inherently present when the beam is applied normal to the substrate [17]. Diamond peaks on the surface can be created by the sputtering of material from the substrate holder or reaction chamber. By tilting the diamond surface with respect to the incident ion beam, these peaks are also angled with respect to the normal of the diamond surface. By subsequently performing a thin etch normal to the surface, the peaks are completely removed. Another problem that can arise from etching at normal incidence is that a deeper etch profile can establish at the edge of etched structures owing to increased etching of an angled face of the mask material (figure 7 a). In order to eliminate this, the surface can be tilted such that the angled face of the mask is normal to the ion beam, and thus etching of the mask is reduced [17] (figure 7 b).

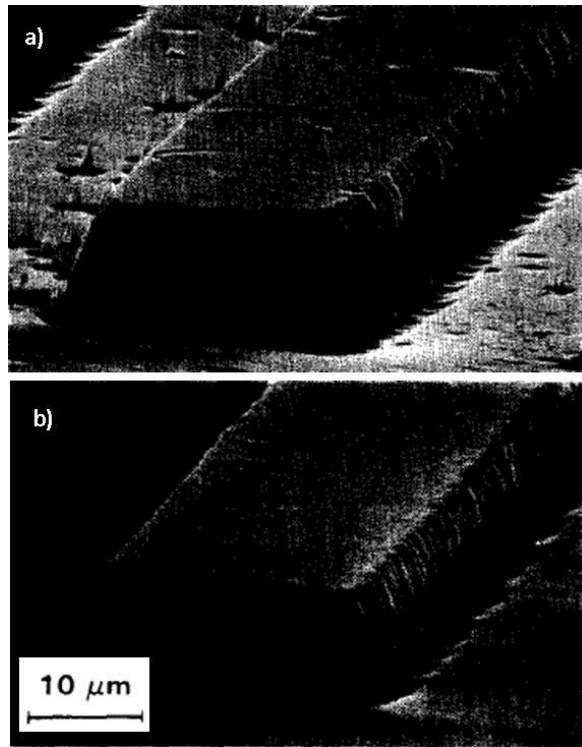


Figure 7 [17]. IBAE of diamond at varied incidence angle: a) with ion beam normal to the substrate, and b) with the ion beam at 45° to the substrate normal.

Varying the angle of incidence in IBAE can also be used to increase the etch rate [19] and to smooth the diamond surface [18]. The level of increase in sputter yield per ion with changing ion beam incidence angle varies depending on the ions involved and their energies (figure 8). As can be seen, an incident angle of approximately 60° from the normal generally results in the greatest sputter yield. Increased ion energy also produces higher sputter yields except in the case of 1000 eV oxygen ions; oxygen ions at this energy are able to penetrate beyond the surface and hence the etching is less efficient, however as the incidence angle relative to the normal is increased, the oxygen atoms still penetrate but the shallower trajectory means that they remain closer to the surface [19].

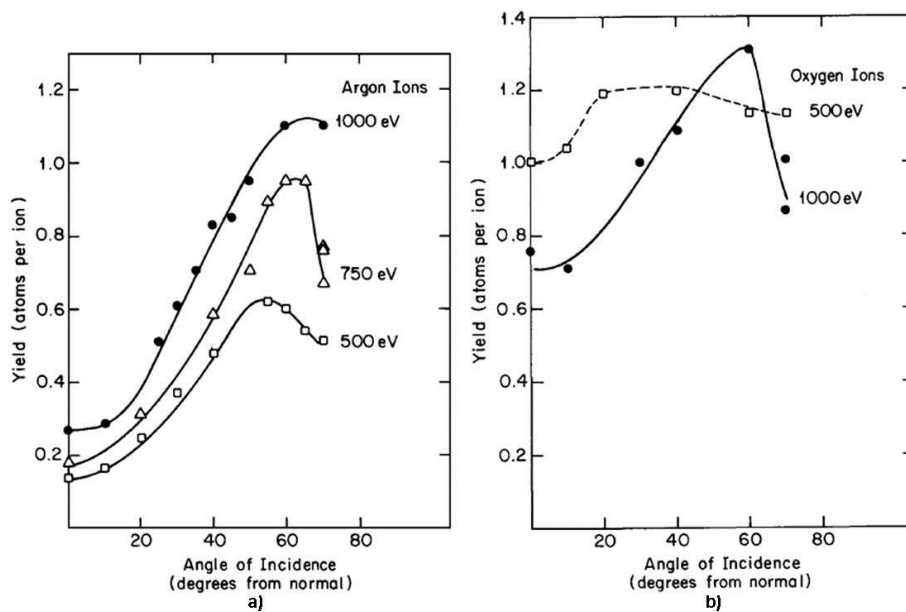


Figure 8 [19] The sputter yield dependence on ion beam incidence angle for diamond etching with, a) argon ions and b) oxygen ions.

## 1.4 Laser methods

Laser ablation proceeds by using a laser pulse to graphitize some of the diamond surface at the incident point, and then subsequently this graphite layer is removed by further laser pulses. Typically, laser pulse frequencies in the nanosecond region are used for this process. However, there are advantages that can be gained from using even shorter frequency pulses in the picosecond and sub-picosecond pulse ranges. Most noticeably, the shorter pulse duration allows lower pulse energies to be used to achieve ablation. This minimises absorption of the pulse energy by the diamond which can otherwise cause graphitization of the area surrounding the incident point and lead to lower resolution diamond patterning [20]. The avoidance of this is seen in femtosecond laser assisted diamond micromachining whereby resolutions up to a quarter of the incident wavelength have been achieved [21]. Another beneficial property of sub-picosecond lasers is that they can be used to study ablation dynamics by using two time-delayed pulses and studying the differences in the surface after each pulse [22].

Laser smoothing of diamond films can be accomplished using direct laser ablation to remove some of the surface diamond. However, this has a severe disadvantage in that the thickness of diamond removed must be greater than the peak-to-trough height in order to achieve a smooth surface. This seriously hinders the practicality of this laser ablation method, owing to the relatively time consuming and costly process of microwave plasma growth of CVD diamond films.

### 1.4.2 Self-Limiting Laser Ablation

An alternative to direct laser ablation uses self-limiting ablation in order to smooth the peaks and troughs in the diamond surface without removal of the base surface. The technique is said to be self-limiting because at a certain point, dependant on several variables, no further ablation occurs.

The diamond surface has an ablation threshold,  $I_{th}(\theta)$ , which is dependent on the laser pulse amplitude,  $I$ , and the angle of incidence of the laser beam relative to the normal to the base plane,  $\theta$  [23]. This technique exploits the dependency on angle of incidence in order to smooth the surface while ensuring that the minimum necessary diamond is removed. The roughness of the diamond surface means that the angle of incidence of the laser beam varies for the base plane and the positively inclined surface peaks (figure 9 a). Therefore, a laser pulse amplitude can be chosen such that the ablation threshold of the positively inclined peaks is reached, but the ablation threshold of the base plane is not reached. Furthermore, the closer the pulse amplitude is to the base plane threshold, the smoother the surface will be before self-limiting occurs.

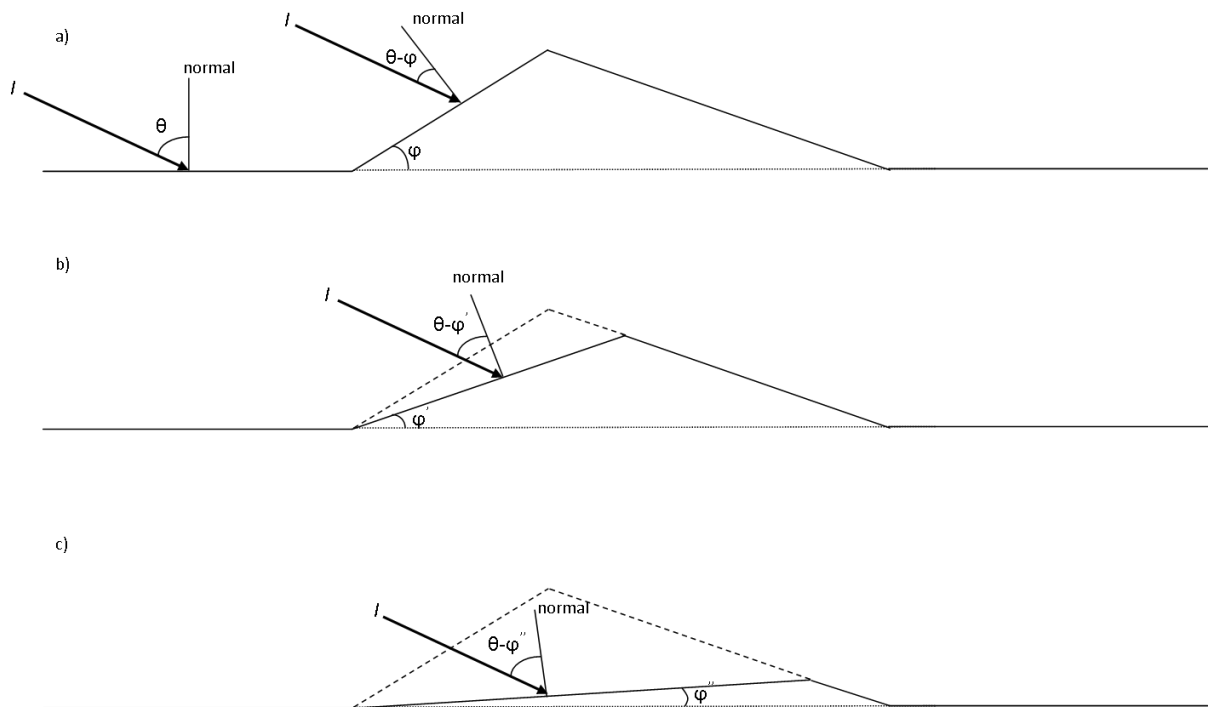


Figure 9 [adapted from 23]. Laser ablation of the diamond surface: a) the difference in relative incident angle of the laser beams for the base plane and positively inclined peak; b) the increasing  $\theta-\phi$  angle as ablation occurs and reduces the peak incline; c) completion of ablation when  $I(\theta-\phi'') = I_{th}(\theta-\phi'')$ .

Figures 9b and 9c show how ablation continues until  $I(\theta-\phi)$  reaches  $I_{th}(\theta-\phi)$  and self-limiting occurs. This leaves a slope with a positive inclination the size of which is dependent on the laser pulse incident angle,  $\theta$ , and the  $I/I_{th}(\theta)$  ratio. Experimental evidence shows that for the most efficient smoothing,  $\theta$  must be greater than  $75^\circ$  and the laser pulse amplitude chosen to be just below  $I_{th}(\theta)$ , i.e. an  $I/I_{th}(\theta)$  ratio of just below 1.

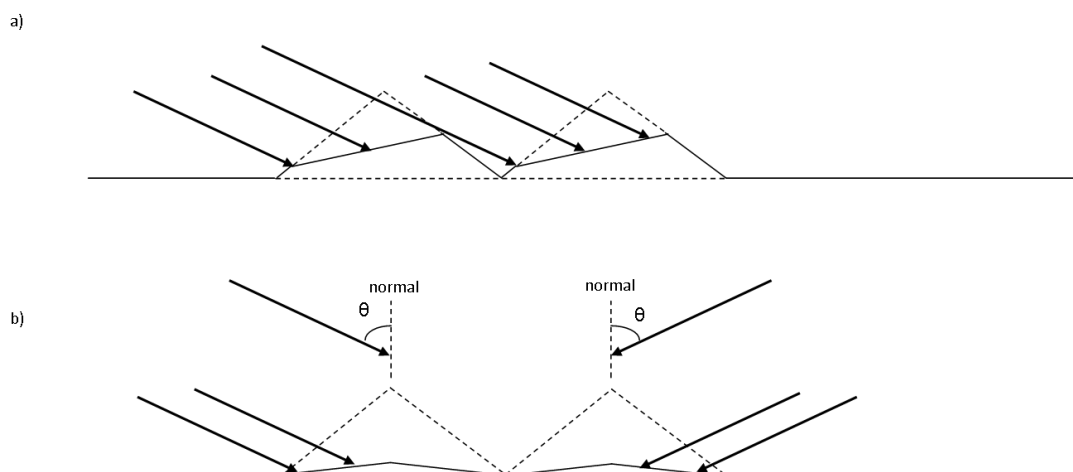


Figure 10 [Adapted from 23]. Laser ablation of peaks on the diamond surface a) without sample rotation meaning shadowing inhibits etching and b) with sample rotation meaning the peak is etched from all sides until self-limitation

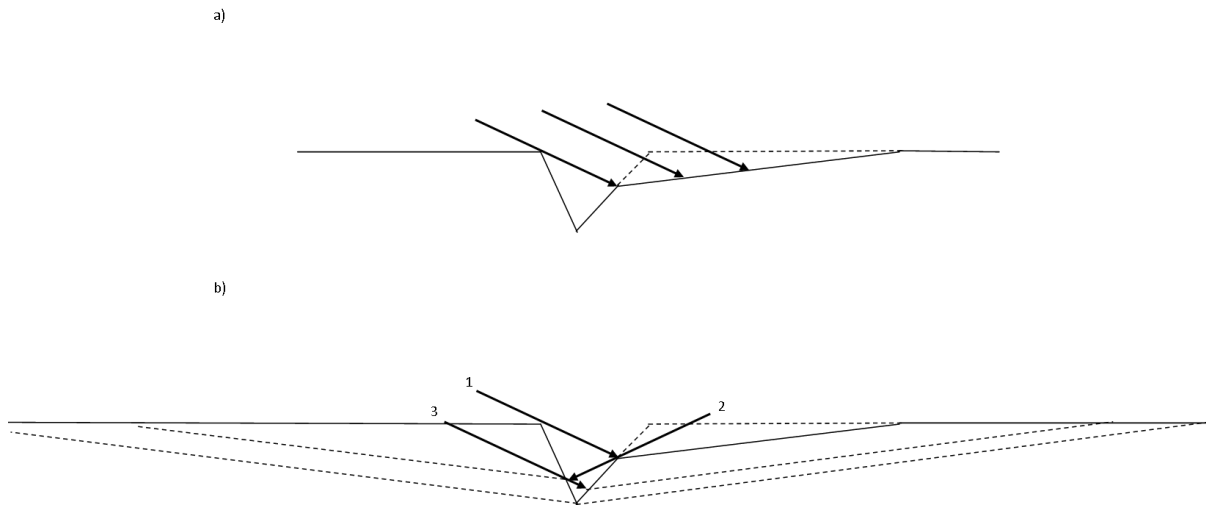


Figure 11 [Adapted from 23]. Laser ablation of pits in the diamond surface, a) without sample rotation meaning shadowing inhibits etching, and b) with sample rotation allowing successive ablation of all of the pit sides

So far only a single surface peak has been considered, and in reality the surface contains many peaks adjacent to each other. This results in shadowing, whereby the incident laser cannot reach the base of peaks meaning the surface is not fully smoothed (figure 10 a). In order to overcome this problem, sample rotation must be employed. The angle of incidence is held constant, but the sample is rotated to allow ablation from all sides (figure 10 b). Smoothing of pits is also aided in this way, as can be seen in figure 11. Sample rotation also avoids the formation of parallel surface channels, which result from irradiation in just one direction.

The combination of sample rotation, incident laser beam angle greater than  $75^\circ$  and laser pulse amplitude slightly less than  $I_{th}(\theta)$  allows the diamond film to be highly polished. Reduction of positive incline peaks to very small angles is possible and this is also achieved efficiently without removal of the bulk through the self-limiting method described. However, a limitation of this method arises in smoothing of pits. Although the pit wall angles can be reduced to very small values, the pit bottom-to-base-plane amplitude remains the same as before ablation. In this regard, direct laser ablation has an advantage because the ablation is not selective and ablation of the base-plane means the valley-to-base-plane amplitude is reduced, albeit at the cost of removing a significant amount of bulk material.

### 1.4.3. Laser Ablation Surface Effects

The atmosphere during the laser ablation process also has an effect on the morphology of the diamond surface and the efficiency of the ablation with respect to etch depth. In the absence of  $O_2$ , a border of graphite remains at the outer edge of the ablation area which is not present in significant quantity when  $O_2$  is present in an atmospheric percentage [24]. In a pure  $O_2$  atmosphere at  $10^5$  Pa pressure, no graphitic sputtered particles are observed in the Raman spectra [24]. This is attributed to the combustion of sputtered particles when oxygen is present. The same principle accounts for the ablation rate in air being higher than a pure  $N_2$  atmosphere and in a pure  $O_2$  atmosphere, the rate is higher again and continues to rise with increased pressure [24].

The presence of a vitreous carbon layer at the diamond surface (characterised by two broad peaks at  $1360\text{ cm}^{-1}$  and  $1580\text{ cm}^{-1}$  in the Raman spectrum [24,25,26]) is relatively uninfluenced by the gaseous atmospheric make-up during ablation [24]. However, when the diamond is ablated under a liquid medium, this layer is significantly reduced (although not completely absent), to the point where a

liquid-etched surface will not conduct electricity, whereas an air-etched surface does[25]. This is owing to the diffusion of heat at the carbon-liquid interface causing the liquid to heat to approximately 2300 K. The removal of the vitreous carbon layer is then achieved because rapid expansion of the high temperature liquid results in a pressure exerted on the carbon layer and hence defacement occurs[25]. However, when short laser pulse frequencies in the picosecond range are used, there is considerably less, if any, carbon remaining. This suggests that at these frequencies, the graphitisation step may be bypassed and the diamond ablated directly [22].

The ablation rate is also dependent on the molecular weight of the ambient gas. This arises because of the reduced flight distance of sputtered particles from collisions with heavier molecules <sup>[Gloor]</sup>. Reduced flight distance means more sputtered particles remain in the etch pits and hence ablation is hindered. This also results in narrower width of surface peaks, because less area is masked by sputtered particles. The dependence of ablation rate on molecular weight can be clearly seen in figure 12. The rate for ablation in a vacuum is significantly higher than for any of the gases shown. This is simply a pressure effect; in a vacuum the plasma formed at the incident site is less dense than at atmospheric pressure, hence the plasma itself absorbs less laser energy and more penetrates to the diamond surface[24]. The ablation rate in liquids is slightly higher than that of air; however, initiation of etching in a liquid medium has a greater time delay than in a gaseous environment [25].

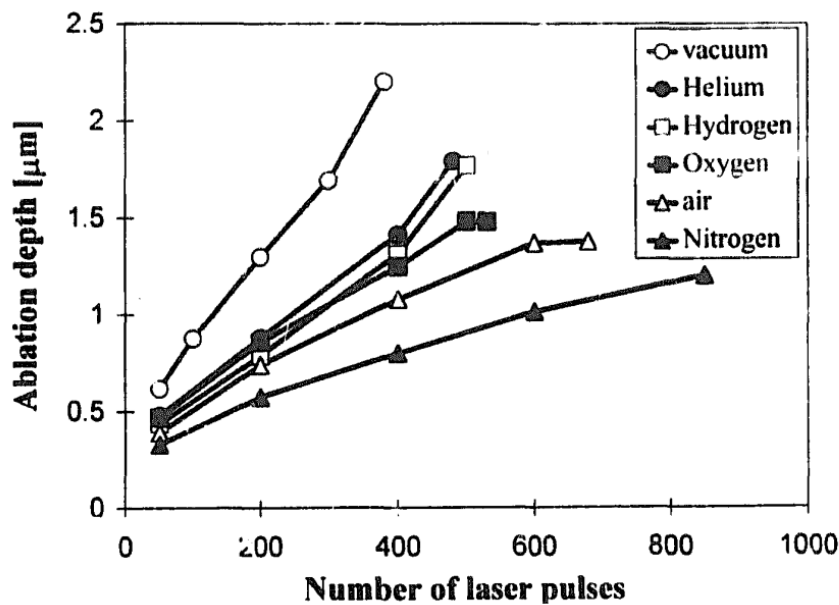


Figure 12[24]. Ablation depth as a function of number of laser pulses for various atmospheres. (ArF excimer laser with  $\lambda = 193$  nm, pulse duration = 20 ns and pulse frequency = 20 Hz).

## 1.5 Diamond Whisker Formation for Field Emission Applications

One of the most significant applications of diamond is its use in electronics. Semiconductors, field emitters and microelectromechanical systems (MEMS) can all benefit significantly from the use of diamond and doped diamond materials. These different applications have individual requirements on the composition and morphology of the diamond resulting in very different approaches to manufacturing the diamond components depending on the specific application.

For field emitter applications, it is desirable to have uniform diamond peaks, or 'whiskers' on the surface. This is owing to the enhanced emission associated with the diamond micro-tip structure [27]. This application is so significant that much research is devoted to it, using many different approaches to achieve a predictable and reproducible diamond whisker pattern.

### 1.5.2 Metal Micro Masks

One way in which diamond whisker formation can be achieved is to use a mask on the surface in such a way that small points on the surface remain un-etched. This has been achieved with reasonable control by depositing molybdenum on the diamond surface and etching with air plasma [28]. The micro mask is created by Mo sputter deposition on the surface which forms randomly distributed clusters of a few nm. This creates an etch-resistant mask by the oxidation of the metal clusters and the reaction of the metal with carbon from the diamond surface to form a metal carbide and hence the clusters remain on top of the diamond whiskers [27]. The whisker formation is achieved by applying a negative voltage bias to the substrate in order to ensure that etching occurs only in the vertical direction and undercutting of the mask is prevented.

This technique successfully results in vertically aligned diamond whiskers with controllable morphologies. The height and thickness of the whiskers may be varied by changing the amount of deposited Mo and the substrate temperature. Increased temperature results in thicker diamond whiskers because the Mo clusters aggregate to form larger clusters and hence protect more of the diamond surface from etching (figure 13). The more Mo deposited, the greater the density of diamond whiskers on the surface; however at a certain coverage, the Mo clusters again become larger resulting in thicker whiskers with lower density [28].

Comparisons between oxidisable and non-oxidisable metals used as the etch-resistant mask in this process have been performed. While non-oxidisable metal masks such as nickel still result in the formation of diamond whiskers, they are reduced in height, have lower diamond quality and form preferentially at grain boundaries in the diamond surface<sup>[L1]</sup>. This is because of the reduced stability of non-oxidisable metals at the diamond whisker tips. Oxidisable metals can react to form a metal oxide or react with carbon to form a metal carbide, and hence create a stable monolayer on the diamond surface. Conversely, non-oxidisable metals do not undergo these reactions and can melt under exposure to a plasma causing them to flow to diamond grain boundaries. Thus, the exact positions of whiskers can be predicted when using a mask such as Mo, but this is not possible for masks such as Ni because the deposited particles can move during etching.

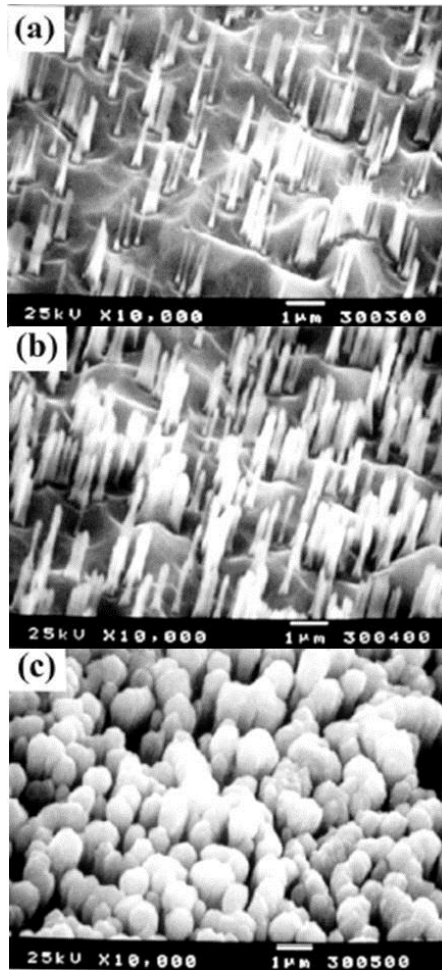


Figure 13 [28] Varying thickness of diamond whiskers formed using a Mo micro mask at different temperatures; a) 300 °C, b) 400 °C and c) 500 °C.

### 1.5.3 Lithographic Techniques

An alternative bias assisted method creates diamond cones on the surface (figure 14) by combining lithographic techniques with an aluminium mask [29]. By exacting control over the level of voltage bias, precise manipulation of the incident angle of reactive ions is achieved and thus the level of side-wall etching is determined. An aluminium mask is placed over the entire diamond surface, and then selectively removed through the use of a photoresist. By making the photoresist layer thicker at specified points, the exact location of diamond cones can be stipulated. A schematic diagram for the method of formation is shown in figure 15.

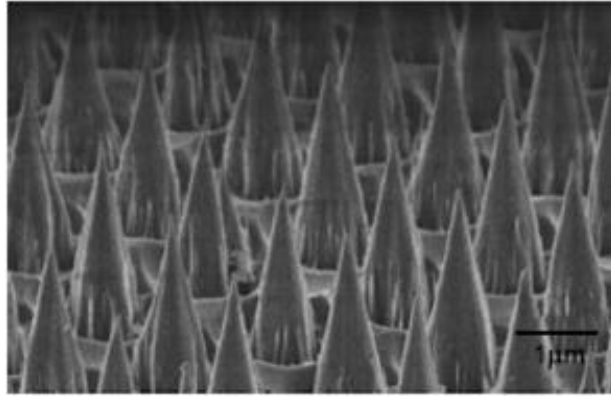


Figure 14 [29]. An SEM picture of diamond cones formed by combining bias assisted etching and lithographic techniques.

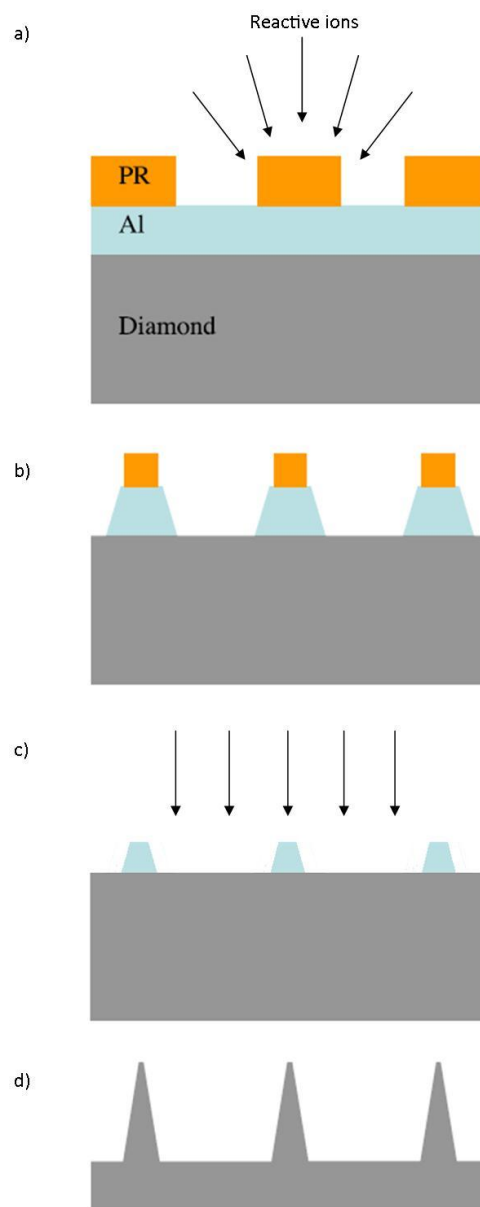


Figure 15 [29]. Schematic process for the formation of diamond cones using lithographic patterning of an aluminium mask.

By the absence of applied voltage bias the incident angle of reactive ions is random, and hence vertical and sidewall etching of the photoresist occur simultaneously (figure 15 a). This results in graduated etching of the aluminium mask as more of the photoresist is removed (figure 15 b). Finally, once the photoresist has been fully etched, a voltage bias is introduced so as to etch exclusively in the vertical direction (figure 15 c) and diamond cones are formed as a result of the graduated aluminium mask (figure 15 d). The diamond cones can be successfully formed down to base diameters of roughly 1  $\mu\text{m}$  and spacing of 1  $\mu\text{m}$ , as well as diamond cone tip radii of just a few nanometres [29].

### 1.5.4 Maskless Etching

A maskless etching mechanism for the formation of diamond whiskers is also possible, potentially simplifying the manufacturing process and reducing the cost. Several techniques have been reported whereby no mask is applied, but sputtering from the substrate holder has led to the creation of micromasks on the surface and hence diamond whiskers are formed [30]. However, it has also been shown that cone formation is possible using a maskless  $\text{H}_2/\text{CH}_4$  plasma etching technique with complete absence of any masking material at the diamond cone tips [16]. It is proposed that this is a result of the rough surface morphology of the CVD diamond film; ion-sputtering is greater at larger angles of incidence, and hence diamond removal is greater at the side of an inherent peak in the CVD diamond film than it is at the top [10,16]. The schematic diagram for this process is shown in figure 16.

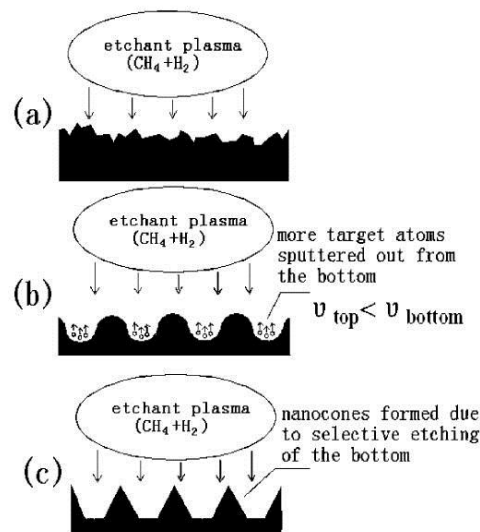


Figure 16 [16]. Schematic for the maskless formation of diamond cones through preferential etching at oblique incidence angle ( $v$  = sputtering rate).

## 1.6 New Methods

The development of a successful technique to consistently produce diamond nanostructures at low cost and in large quantities would have very wide applications, ranging from electrical to biochemical uses. Therefore, significant research in this area is on-going, with new approaches being employed to achieve high resolution diamond structures.

Recently, a new masking technique has been developed which allows better resolution and sidewall angle control under etching [31]. This is achieved through the use of a gallium focused ion beam

(FIB) to pattern the diamond surface with a dry etch mask prior to etching with a plasma (figure 17 (a) and (b)).  $\text{Ga}^+$  ions, of energy below that required for ion milling, are implanted in the diamond surface which leads to the creation of an amorphous carbon and gallium (a-C/Ga) layer on top of the diamond surface. This layer shows good resistivity to both chemical and physical etching pathways, with diamond : a-C/Ga selectivity of 100 : 1 being achievable [31]. This resistivity means the technique may be applied across a range of plasmas including both oxygen and argon plasmas.

A significant advantage of this technique is the ease with which the patterning of specific structures can be achieved. The direct-write method allows nano-scale structures to be easily created with good resolution (figure 17 c), as well as the possibility for larger areas of masking (figure 17 (d) and (e)).

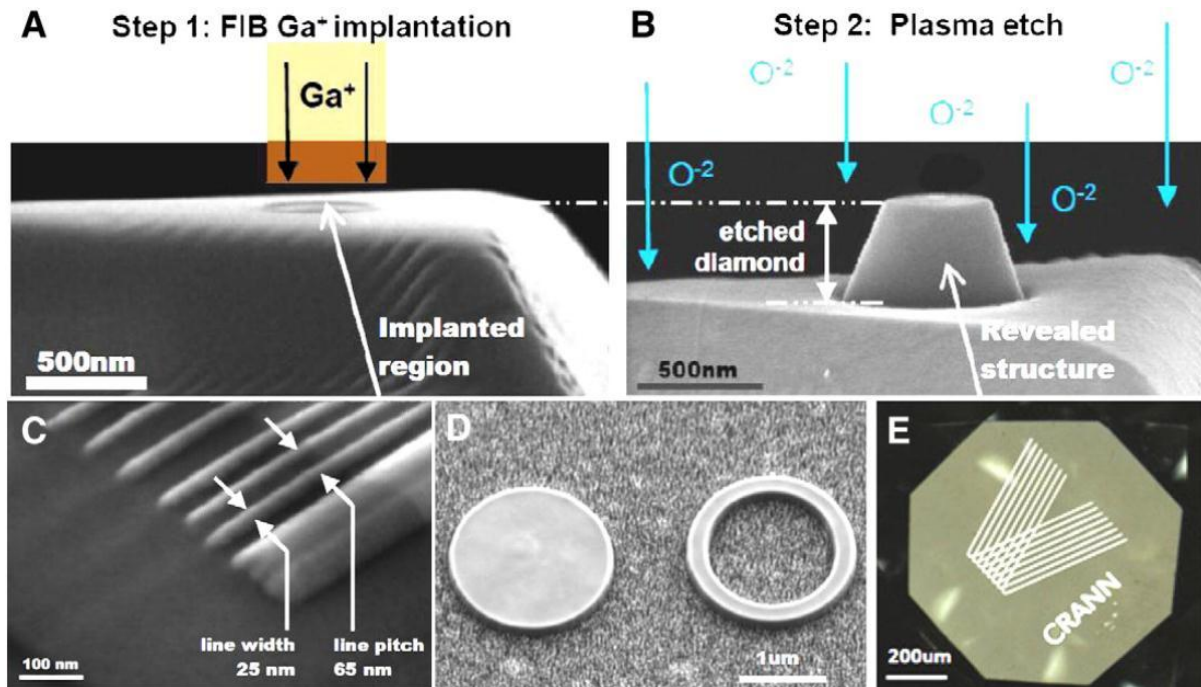


Figure 17 [31]. Gallium FIB diamond masking: A) gallium ions implanted into the diamond surface creating a direct write mask. B) oxygen plasma etching of the masked surface results in a nanostructure on the diamond surface. C) nano-scale lines formed on a single crystal diamond surface. D) micro-scale structures etched into a diamond on silicon film. E) a large area (approximately  $1\text{mm}^2$ ) pattern etched on a facet of a natural diamond.

Currently, this technique is limited by the absence of a satisfactory method for mask removal after etching. The mask layer thickness can be determined through control of the voltage used in FIB implantation, and this allows for control of the etching such that on reaching the required etch depth, the mask has also been removed [31]. However, this is sometimes not possible and complicates the procedure, so a more reproducible mask removal technique is required.

Another recent method for masking diamond prior to etching uses a metal film coating, which is then exposed to a plasma and leads to the creation of nanoparticles on the surface [32]. Subsequent RIE of the surface yields different diamond surface morphologies dependent on the mask material. When a nickel metal layer is applied, the process results in the formation of diamond nano-rods (figure 18 a) due to the resistance to etching of the nickel nanoparticles. A gold nanoparticle mask gives an uneven “cauliflower” type nanostructure to the surface (figure 18 b). The diamond nano-rod formation resulting from the nickel mask is not observed because whilst initially etching of the diamond surface under the gold particles is inhibited, the gold particles are not as resistant to etching as the nickel particles.

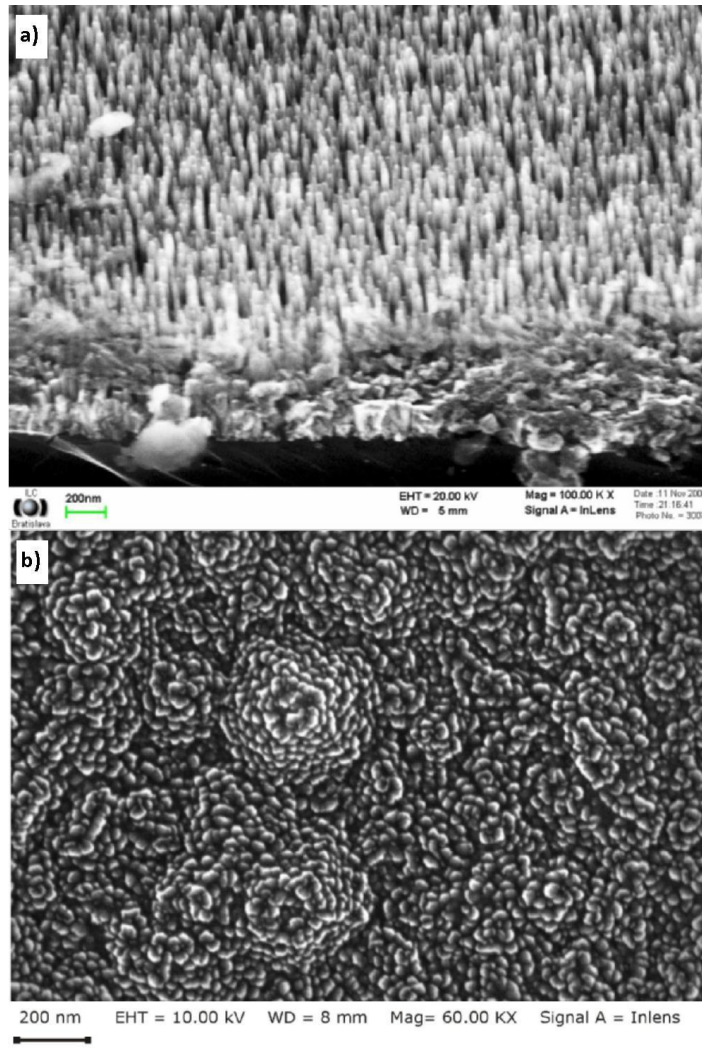


Figure 18 [32]. Diamond surface morphology after RIE in the presence of a metal mask; a) tilted view of the nano-rods formed as a result of a nickel mask, and b) top view of the surface after etching with a gold mask.

A similar technique also involves the creation of nickel nanoparticles on the surface, however the etching of the diamond is then achieved by the nanoparticles themselves leading to the creation of etch pits in the diamond surface [33]. A layer of nickel is deposited on the diamond surface and then heated in a low pressure hydrogen atmosphere until melting occurs. The temperature required is lower than the melting point of nickel; this is owing to both the diffusion of hydrogen into the metal and the reduction of melting point associated with thin metal films [34]. The melting of the nickel film results in the formation of nickel nanoparticles with an average diameter of approximately ten times the original thickness of the metal layer. The high temperature and low pressure conditions are then maintained, resulting in etching of the diamond surface. Etching times at 1000°C and 500 mbar hydrogen pressure are roughly 90 minutes, however the etch rate increases with increased temperature and hydrogen pressure.

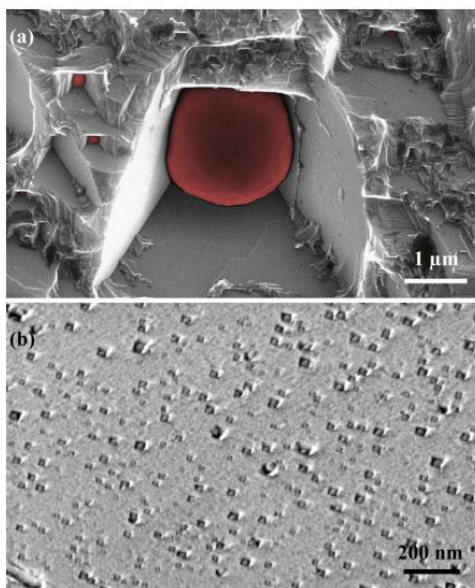


Figure 19 [33]. SEM photographs of the etch pits created in CVD diamond by hot nickel particle etching:  
a) close up of etch pit created by a large micron scale Ni particle and, b) the diamond surface after etching with smaller Ni nanoparticles.

The etching of the diamond through this method is accomplished through the chemical interactions of the diamond and nickel. The interactions between the diamond and hot nickel nanoparticle interface are believed to convert the diamond to non-diamond carbon. This is then able to diffuse into the nickel, and subsequent reactions with hydrogen result in the formation of methane and other hydrocarbons[33]. Despite the spherical structure of the nickel nanoparticles, straight edged ‘square’ shaped etch pits are formed when etching CVD diamond films (figure 19). However, the surface morphology is heavily dependent on the diamond plane being etched when using this process with single-crystal diamonds. The etching of the {111} diamond plane is shown to be slower than the other planes and hence the etching is restricted when the nickel nanoparticle reaches these planes. Therefore, the orientation of these planes with respect to the etching direction determines the shape of the etch pit formed. The different shaped etch pits for different crystal planes are shown in figure 20.

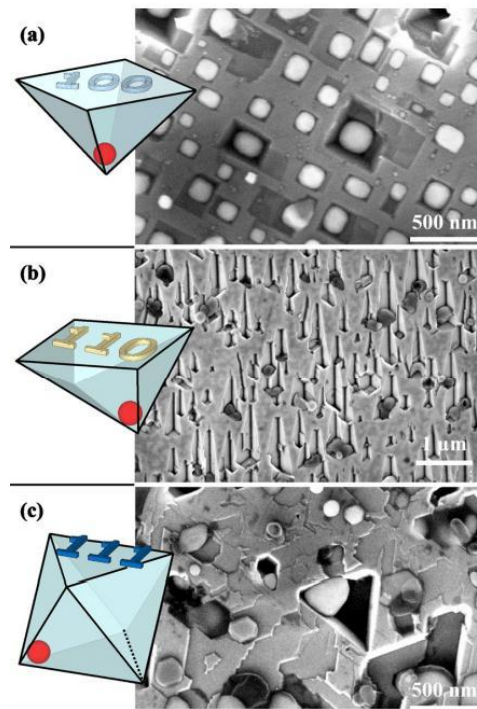


Figure 20 [33]. SEM micrographs of the etch pits observed in different single crystal diamond planes: a) {100}, b) {110} and c) {111}. The inserts show the shapes of the etch pits formed due to restricted etching at the {111} plane boundaries. All the faces are {111} except the otherwise labelled top faces, and the red circle indicates the Ni particle at the bottom of the etch pit.

This technique has also been carried out using different metal nanoparticles to etch a highly {100} – oriented diamond coating ({100}HODC) [35]. Very similar results were reported, with the etch pits being shaped by the presence of {111} planes. Table 1 shows a summary of the various results from etching with different metals at a range of temperatures.

Table 1 [35]. Summary of the etching outcome of different metal nanoparticles on {100}HODC

Specimen	Treatment temp.	Form of metal particles	Surface morphology of {100}HODCs
{100} HODC			<ul style="list-style-type: none"> <li>• Flat surface with steps</li> <li>• Neither etch pits nor nano-channels</li> </ul>
Fe- $\{100\}$ HODC	800 °C	<ul style="list-style-type: none"> <li>• Distorted round-shaped particles bulging out from their respective etch pit sites</li> </ul>	<ul style="list-style-type: none"> <li>• Neither nano-channels nor etch pit sites except near the edge part of Co-<math>\{100\}</math>HODC</li> </ul>
	900 °C	<ul style="list-style-type: none"> <li>• Same as at 800 °C</li> </ul>	<ul style="list-style-type: none"> <li>• Etch pits with Fe particles</li> <li>• Vacant etch pits were also observed</li> </ul>
Co- $\{100\}$ HODC	700 °C	<ul style="list-style-type: none"> <li>• Small round-shaped particles</li> </ul>	<ul style="list-style-type: none"> <li>• Almost the same as at 800 °C</li> </ul>
	800 °C	<ul style="list-style-type: none"> <li>• Square particles with round corners at etch pits or at the end of short nano-channels</li> </ul>	<ul style="list-style-type: none"> <li>• Etch pits with Co particles</li> <li>• Short nano-channels</li> </ul>
	900 °C	<ul style="list-style-type: none"> <li>• Almost the same as at 800 °C</li> </ul>	<ul style="list-style-type: none"> <li>• Vacant etch pits were also observed</li> </ul>
Ni- $\{100\}$ HODC	800 °C	<ul style="list-style-type: none"> <li>• Almost the same as the case in the Co-HODC</li> </ul>	<ul style="list-style-type: none"> <li>• Almost the same as the case in the Co-<math>\{100\}</math> HODC</li> </ul>
	900 °C	<ul style="list-style-type: none"> <li>• Almost the same as the case in the Co-HODC</li> </ul>	<ul style="list-style-type: none"> <li>• Almost the same as the case in the Co-<math>\{100\}</math>HODC</li> </ul>
Pt- $\{100\}$ HODC	900 °C	<ul style="list-style-type: none"> <li>• Small round-shaped particles</li> </ul>	<ul style="list-style-type: none"> <li>• No evidence of etching by Pt particles</li> </ul>
	1000 °C	<ul style="list-style-type: none"> <li>• Round-shaped particles</li> </ul>	<ul style="list-style-type: none"> <li>• Etch pits with Pt particles</li> </ul>

Another technique for etch pit formation employs a defected silicon nitride layer over the diamond surface [36]. The defects are created by application of a photoresist and subsequent RIE. Defects

inherent in the photoresist layer are ‘transferred’ to the silicon nitride layer by this RIE, creating holes in the silicon nitride surface. Removal of the photoresist followed by further etching under water and molecular oxygen gas flow results in square etch pits in the diamond surface (figure 21).

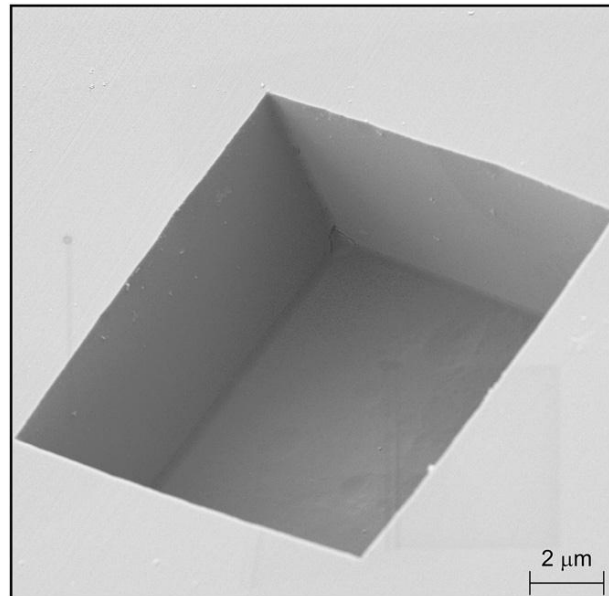


Figure 21 [36]. SEM micrograph of an etch pit formed in the diamond surface. The pits formed are approximately square, with a depth of roughly half the width.

The size of the etch pit formed is proportional to the size of the initial silicon nitride hole, with a larger hole in the surface allowing for a faster flow of gasses and hence a faster etch rate. The consistent geometry of the etch pits suggests a limiting boundary to the etching process. It is believed to be the slow etching {100} planes that are responsible for the smooth scale-similar nature of the pits.

## 1.7 Microelectromechanical (MEMS) Applications

Diamond has excellent potential for use in microelectromechanical (MEMS) applications. Therefore, a significant proportion of diamond based research is focused on developing techniques for the fabrication of diamond micro-devices. Several techniques can be employed for this objective, although RIE has an inherent advantage because it allows better etching direction control compared to other etching techniques. However, achieving patterns that are smooth, straight and accurate enough for MEMS applications proves difficult.

A RIE technique that seeks to improve the quality of fabricated structures utilises sidewall passivation through mask sputtering[37]. A metal mask is applied across the entire diamond surface prior to applying a photoresist and chemically etching to remove some of the metal layer and leave just the desired etch pattern masked. As RIE in an oxygen/argon plasma involves both chemical and physical etching pathways, some sputtering of the mask occurs as well as etching of the unmasked diamond. Sputtering of the metal then leads to the formation of a metal oxide, which is then re-deposited around the area of etching, including the sidewalls and bottom of the freshly etched pit (figure 22).

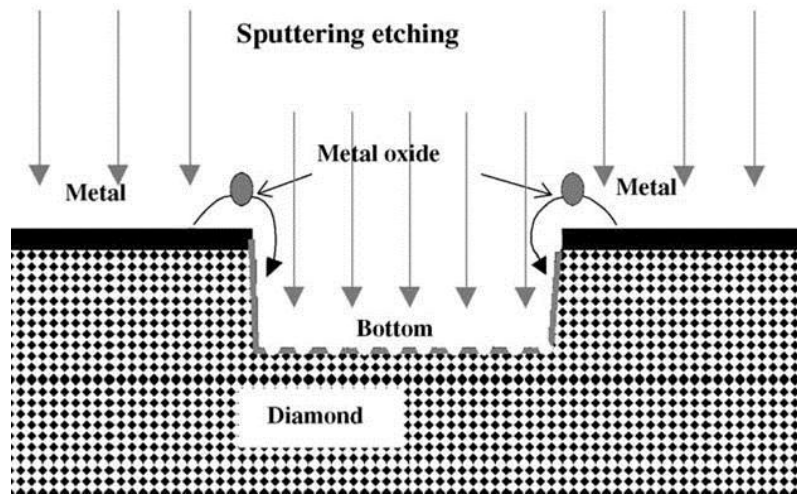


Figure 22. [37]. Model for sidewall passivation under RIE in an etching environment with both chemical and physical pathways.

Although the metal oxide layer is deposited on the bottom of the etch pit as well as the side walls, further vertical etching is not inhibited. This is owing to the anisotropic nature of physical sputtering etching; the metal oxide layer at the bottom of the etch pit continues to be sputtered allowing chemical etching of the diamond to continue in the vertical direction, while side wall etching is restricted.

Careful control of the etching conditions are required to maintain the sidewall passivation; the ratio of chemical : physical etching pathways and the vacuum pressure are the most important variables to consider. Under the correct conditions, this technique can successfully fabricate accurate and straight edged devices of micro-scale (figure 23).

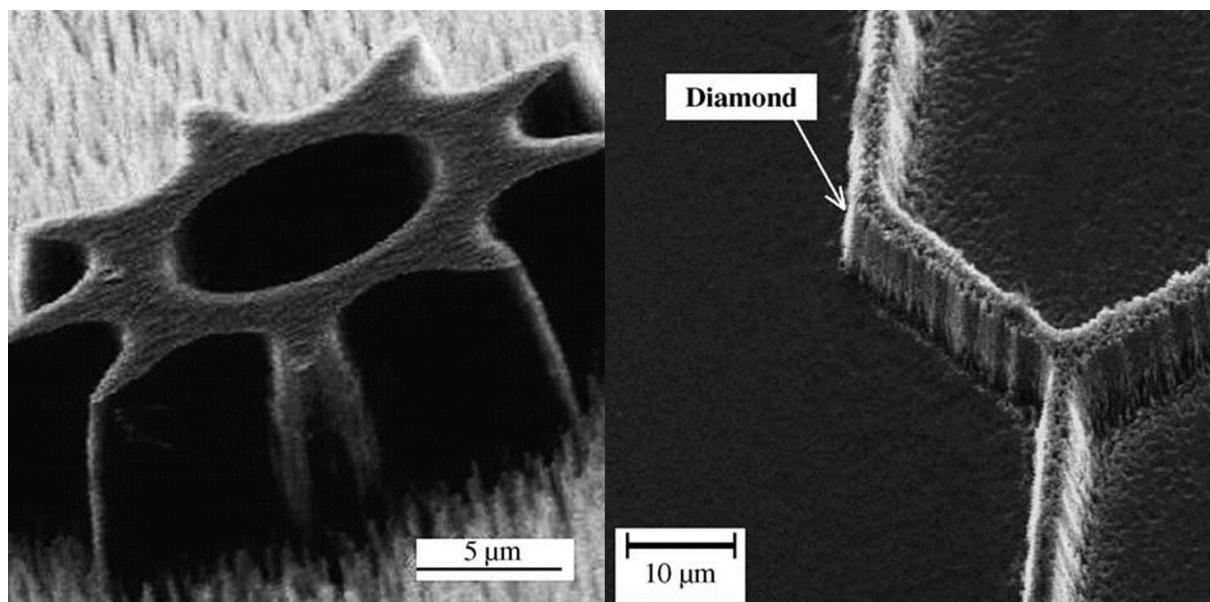


Figure 23 [37]. SEM pictures of diamond micro structures etched by RIE employing the sidewall passivation method.

## 1.8 Research Focus

This particular research is directed towards the formation of diamond whiskers. As discussed in section 1.5 above, a major area of application for these diamond nanostructures is for use as thermionic emitters in microelectronic devices. In addition to this, the resultant increased surface area of the diamond film enables their employment in hydrogen storage applications. Hydrogen is becoming increasingly significant as an alternative fuel source. However, hydrogen's attractive high energy to weight ratio is compromised considerably by its poor energy to volume ratio (figure 24). Thus hydrogen storage solutions are an area of intensive research.

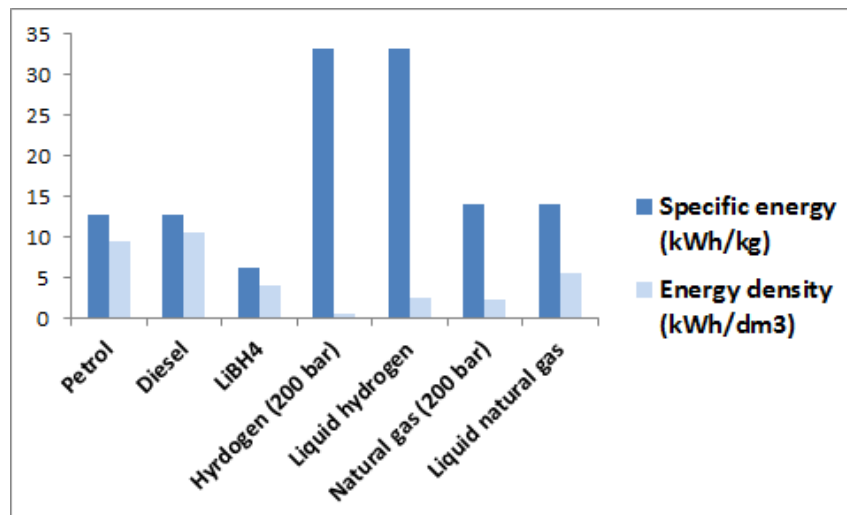


Figure 24 [Adapted from 38]. A comparison of the specific energies and energy densities for some common fuel sources.

The relevance of diamond films in this field is a result of hydrogen's known ability adsorb to the surface of diamond, as well as rapidly diffuse into the bulk of the diamond material [39]. As well as maximisation of the grain boundaries within diamond film, surface area maximisation has potential to increase the efficiency with which hydrogen is adsorbed / absorbed.

Therefore, the aim of this research is to investigate the formation mechanism of diamond whiskers; a view to optimising the formation of uniform, predictable and reproducible structures, as well as maximising the surface area increase is employed.

## 2. Experimental

Both the polycrystalline CVD diamond film and boron doped ( $10^{20} \text{ cm}^{-3}$ ) polycrystalline CVD diamond film used in this research were purchased from element6.

The following acid cleaning process was performed on all samples prior to etching. 100ml of sulphuric acid was degassed by heating at 120 °C for 2 hours. The diamond samples were added into the reaction flask before nitric acid was generated in situ by addition of 6.5g of potassium nitrate. This was then refluxed for 2 hours at 200 °C.

UV and visible Raman spectra were taken of both boron doped and undoped films before and after acid cleaning treatment. The exposure time was 10s and the result was averaged over 10 accumulations.

Direct current (DC) plasma etching was performed on both boron doped and undoped samples. Gas mixtures of argon/hydrogen (1:1), argon/oxygen (4:1) and air were all used at a pressure of 50 mtorr. Samples were placed on a DC magnetron cathode, biased at 2.5kV. The DC plasma treatment was carried out at a power of 150W for a duration of 20 minutes. A second plasma etch was carried out on the boron doped diamond samples, using the same plasma conditions and reactant gases as the first etch, however the etch duration in this second cycle was increased to 40 minutes.

Surface characterisation and surface morphology investigation were carried out by Raman spectroscopy and field emission gun scanning electron microscopy (FEGSEM) (JEOL JSM 6330F / Helios Nanolab Dual Beam 600i).

## 3. Results and Discussion

The Raman spectra for undoped and boron doped diamond films before and after acid cleaning treatment are shown in figure 25. From the broad peak at  $1580 \text{ cm}^{-1}$ , it is clear that in both cases some level of  $\text{sp}^2$  carbon remains present after cleaning. As discussed in section 3.2 below,  $\text{sp}^2$  carbon may possibly be influential in the formation of nanostructures. Thus, this presence must be considered to have an effect on the overall results, and further investigation would be required in order to qualitatively determine the effect this has on the resultant surface morphology.

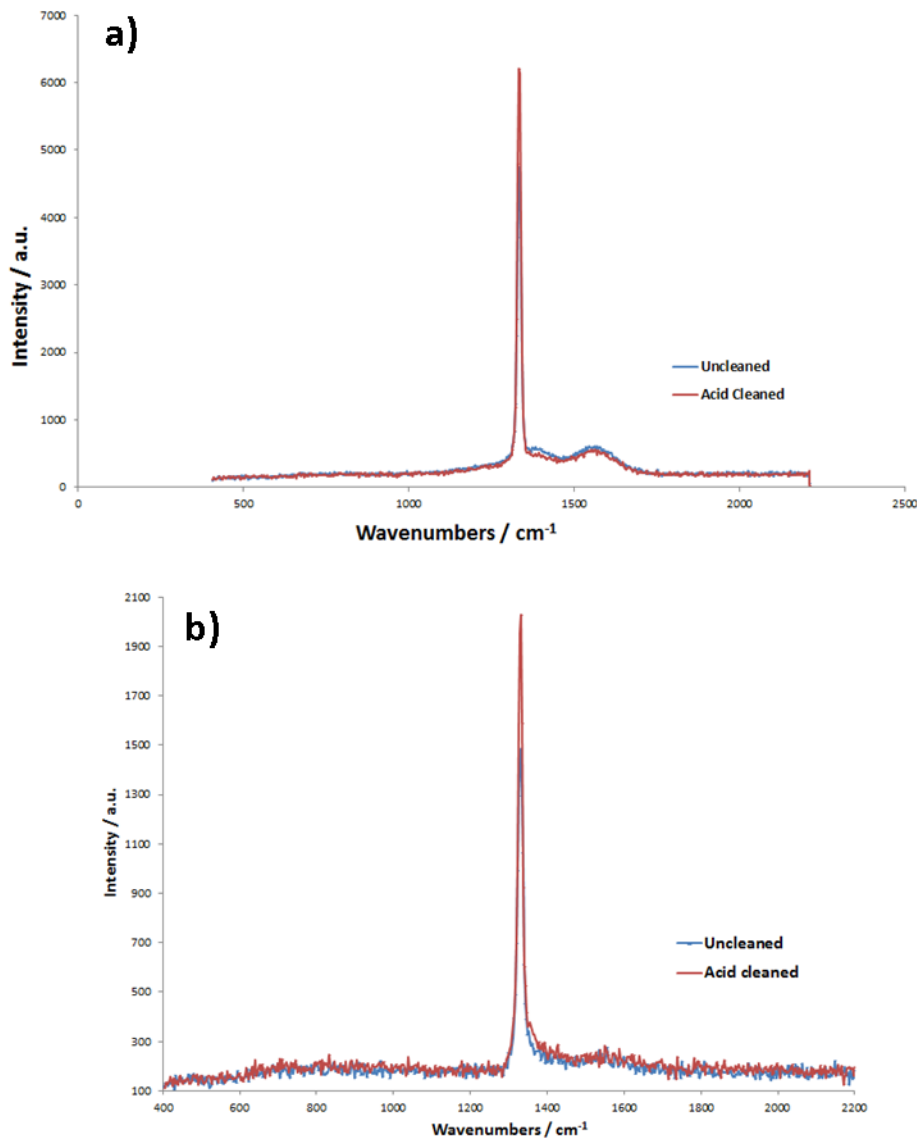


Figure 25. UV Raman spectra of diamond films before and after acid cleaning treatment; a) undoped and b) boron doped.

## 3.2 Undoped Diamond Films

### 3.2.1. Formation Mechanism

As discussed, the morphology of the etched diamond surface is dependent on the gas mixture used, owing to the relative contributions of physical and chemical etching pathways.

For the oxygen/argon plasma etch, predominantly chemical etching by oxygen ions is combined with purely physical etching by argon ions [27]. The effect on etch rate of increasing the percentage of O<sub>2</sub> in the gas mixture has been inconsistently reported in the literature. Increase, no change and decrease of etch rate with increasing O<sub>2</sub> concentration have all been reported [9,19,27], however the gas chamber pressure was significantly higher in the latter case. This suggests that as well as the overall

etch rate, the relative proportions of etching processes involved may be dependent on gas chamber pressure.

In terms of the morphology of the surface after etching, increased percentage of oxygen has been shown to result in higher density of diamond whiskers [27]. At low oxygen/argon ratios, whiskers are only present at grain boundaries. This is considered to be a result of higher presence of non-diamond  $sp^2$  carbon at grain boundaries [27, 40]. Increased electric field concentration due to graphite conductivity is responsible for localised ion bombardment at grain boundaries [8]. It is also suggested that this effect is in part due to the higher density of {111} facets present at the grain boundaries, which have been shown to etch preferentially over other diamond crystal faces [41].

A similar effect is seen for pure oxygen etching of diamond films; an oxygen pressure below approximately 5 Pa is insufficient to produce uniformly distributed diamond whiskers, however increasing the pressure to above 5 Pa results in evenly distributed whiskers with good uniformity [41]. The same dependence on pressure has been shown to be true of heavily boron doped diamond films [42]. This dependence on ion pressure is due to reduced kinetic energies of ions at higher pressures [42]. Equation (1) [43] shows how the average energy of the ions at the surface,  $\bar{E}$ , is dependent on the ion mean free path,  $\lambda$ , which decreases with increased ion number density,  $n$ , as shown in equation (2) [43].

$$\bar{E} = e V_0 \left[ 1 - \left( 1 - \frac{\lambda}{ps} \right)^2 \right] \quad (1)$$

$$\lambda = \frac{1}{\sigma n} \quad (2)$$

The formation mechanism of diamond whiskers by etching of CVD diamond films is a continued area of research, and in no way fully understood. As discussed in section 1.5.2 above, many literature examples employ an etch resistant mask sputtered onto the diamond surface, resulting in whisker tips coinciding with the positions of mask material. While the positioning of diamond whiskers in these examples is intuitive, the preferential whisker formation at grain boundaries when low pressures are used is not fully understood. Low pressure etching gas has been shown to sputter a uniform spread of mask material from the substrate holder, yet selective whisker formation at grain boundaries is observed [41]. It is likely that this effect is a result of the same processes as those occurring in the whisker formation by maskless etching of diamond films.

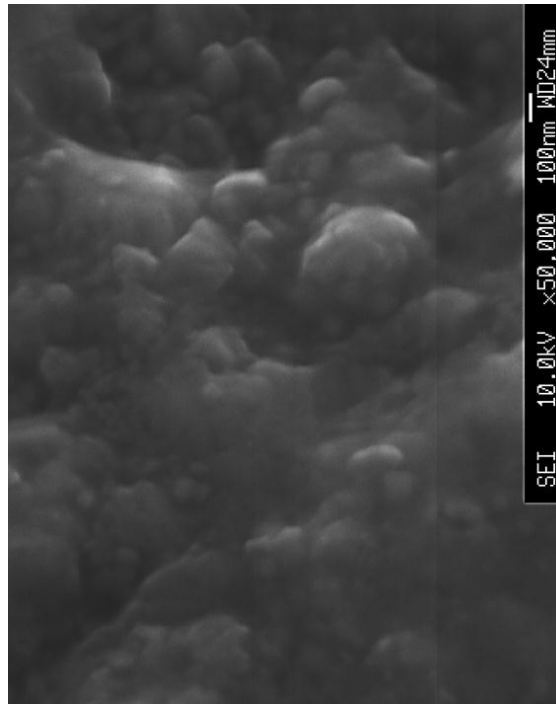


Figure 26. FEGSEM micrograph of Ar/H<sub>2</sub> DC plasma etched undoped diamond film.  
The image was taken at a perspective tilt angle of 40° normal to the surface.

Figure 26 shows the resultant surface morphology after etching undoped diamond film with an Ar/H<sub>2</sub> DC plasma. As can be seen, selective localised etching has resulted in smooth, rounded surface nodules. This is in significant contrast to the structures observed from etching with an Ar/O<sub>2</sub> bath gas (figure 31). This smoothing effect is expected of hydrogen based gas mixtures, due to the known ability of hydrogen to polish the diamond surface [44]. The formation of structures on the surface rather than an overall polishing effect is attributed to the presence of oxygen ions; with pure H<sub>2</sub> etchant gas only the chemical etching pathway is available, however, addition of oxygen means physical sputtering etching also contributes to the etching process.

This result differs from the uniform diamond cone array achieved from hydrogen plasma etching described in reference [16]. This is attributed to the employment of a less powerful etching technique in this research. The substrate temperature of 900°C coupled with a substrate bias of -350V in the mentioned example, as well as longer etching durations, account for the significantly different surface morphology. It is reasonable to assume that these conditions would result in a degree of anisotropic etching, compared to relatively isotropic etching under the milder conditions employed in this research. Hence, in this case, while structure formation is observed, there is simultaneously a smoothing of the diamond surface.

### 3.2.2 Raman Spectra Comparison

Figure 27 shows the Raman spectrum of the diamond film etched in a hydrogen and argon gas mixture. As indicated by the prominent graphitic peak at 1580 cm<sup>-1</sup>, there is still a significant presence of sp<sup>2</sup> carbon post etching. As it is unlikely for the original graphitic material would remain after etching, the implication is that graphitic material is produced during etching. This is consistent with the etching pathways available when using the Ar/H<sub>2</sub> gas mixtures: as argon etches the diamond through forming physical defects and converting diamond material to graphite, hydrogen removes the graphitic material through a chemical pathway. The inference here is that the overall etching pathway must be more physical than chemical, as an equilibrium amount of graphitic material remains present [8].

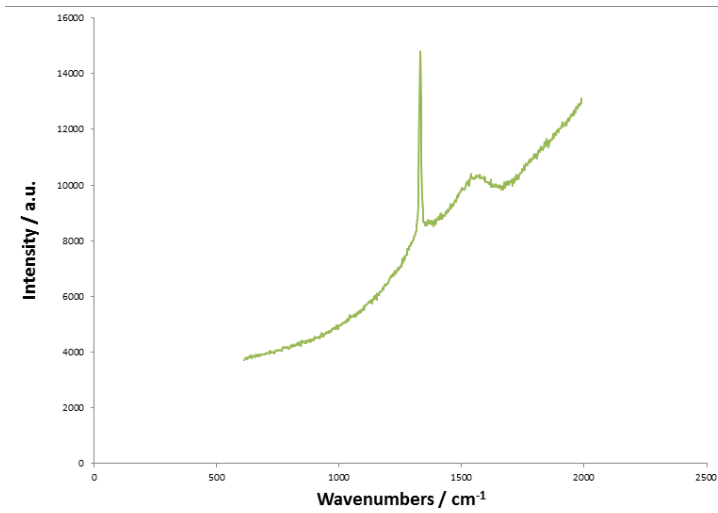


Figure 27. The visible Raman spectrum of undoped diamond film etched in Ar/H<sub>2</sub> plasma.

A very similar result is observed for the etching in air and Ar/O<sub>2</sub> gas mixtures, as shown in figures 28 and 29 respectively. This is also as expected for the etching processes involved, with argon etching via a purely physical pathway and oxygen through both physical and chemical. It is important to note that although the presence of sp<sup>2</sup> carbon can be confirmed for all of the undoped samples, no qualitative data can be extracted from the Raman spectra, and further analysis would be required to determine the relationship between etching pathways involved and the extent of resultant graphitic carbon.

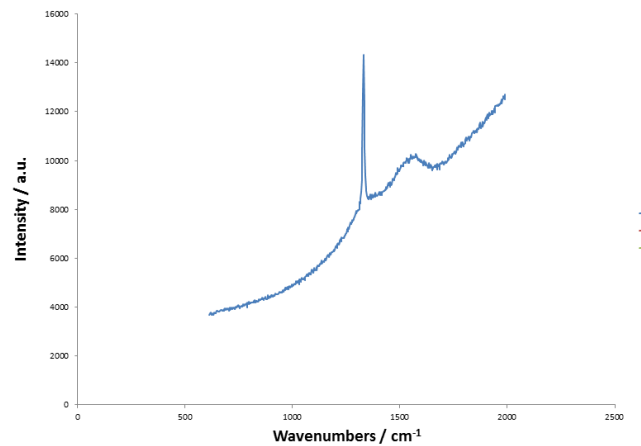


Figure 28. The visible Raman spectrum of undoped diamond film etched in air plasma.

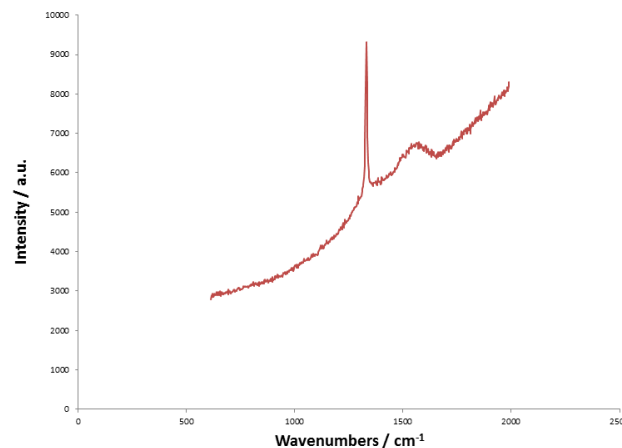


Figure 29. The visible Raman spectrum of undoped diamond film etched in Ar/O<sub>2</sub> plasma.

### 3.2.3 Effect of Etching Gas

The surface morphology resulting from air etching (figure 30) is comparable to that of Ar/H<sub>2</sub>. However, the density of surface structures is evidently much greater than with an argon hydrogen gas mixture. It is possible that the lower density of structures when H<sub>2</sub> is present could be due to the polishing effect of hydrogen effectively smoothing structures together, or removing smaller structures completely, but this is unlikely considering the relatively short etching duration and other factors certainly contribute.

The kinetic energy of ions in a plasma affects the surface morphology due to the increased etch rate resulting from a greater number of defects being created [8]. The average kinetic energy of ions being greater in the air plasma than in the Ar/H<sub>2</sub> will therefore effect the surface morphology. Potentially it may be this increased density of defects that leads to a higher density of structures.

The high percentage of nitrogen present in the air plasma is likely to have an effect. Despite the high chemical inertness of nitrogen, it is reasonable to envisage that under the severe plasma etching conditions, nitrogen will contribute and have an effect on the resultant surface morphology. The extent of the contribution of nitrogen is difficult to extract in this case because the etching rate of oxygen plasmas is known to be relatively high [9]. However, a comparison between the etching result for air plasma and that of an Ar/O<sub>2</sub> plasma allows for some inferences to be made, based on the fact that argon etches via a purely physical pathway.

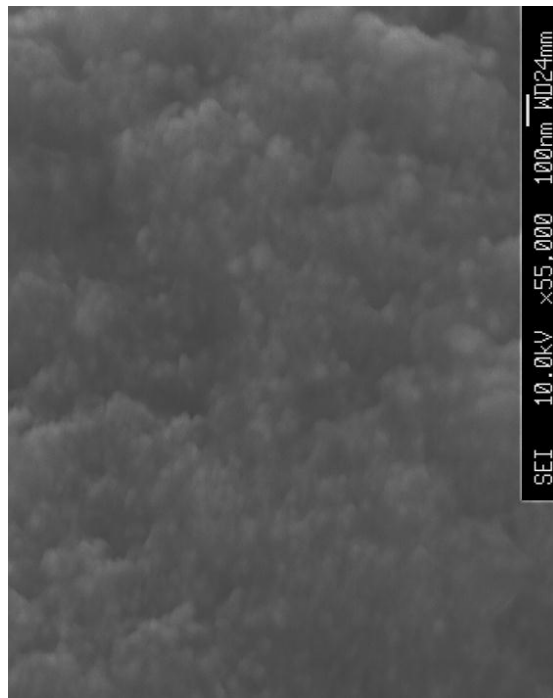


Figure 30. FEGSEM micrograph of air DC plasma etched undoped diamond film. The image was taken at a perspective tilt angle of 40° normal to the surface.

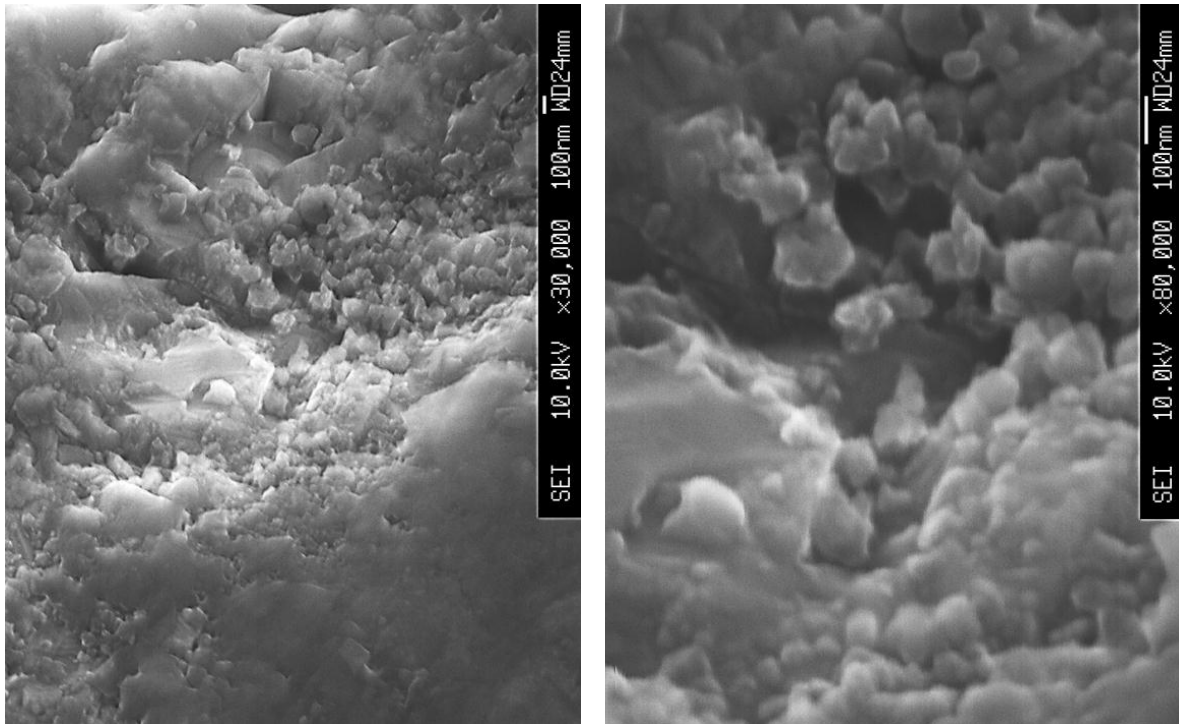


Figure 31. FEGSEM micrographs of Ar/O<sub>2</sub> DC plasma etched undoped diamond film.  
Both images were taken at a perspective tilt angle of 40° normal to the surface.

The result of etching undoped diamond film with an Ar/O<sub>2</sub> gas mixture (figure 31) is decidedly different from the previous examples. The density of structures formed appears similar to that in the case of air etching (figure 30). However, a significant difference in this case is that the structures formed are less polished, having slightly sharper features.

It has been reported in the literature that argon/oxygen gas mixtures have a relatively high surface roughening effect compared with other etching gas mixtures [9]. The surface formed in this experiment however is inconsistent with the findings ref [9] where nodular structures were formed only with pure O<sub>2</sub> gas, and the presence of argon led to a smoothing of the surface. This discrepancy is most likely due to the weaker etching conditions and shorter etch duration used in this experiment.

It has been shown that etching with pure argon gas does not lead to surface structure formation [27], and that Ar/O<sub>2</sub> gas etches through diamond to graphite conversion by reactive ions [8], followed by removal of this graphitic carbon through volatile product formation from reaction with oxygen radicals [27]. Thus, it must be considered that the ratio of Ar/O<sub>2</sub> will have a significant effect on the etching process itself as described in reference [9], and this will consequently influence the surface outcome.

Therefore, it must be realised that the direct comparison of results with those in the literature is delicate, and small changes in etching conditions may have a substantial effect. Thus, in order to fully appreciate the effects of the different etching gases used here, further enquiry is needed to provide results that are quantitatively comparable.

## 3.3 Boron Doped Diamond Films

### 3.3.1 Raman Spectra Comparison

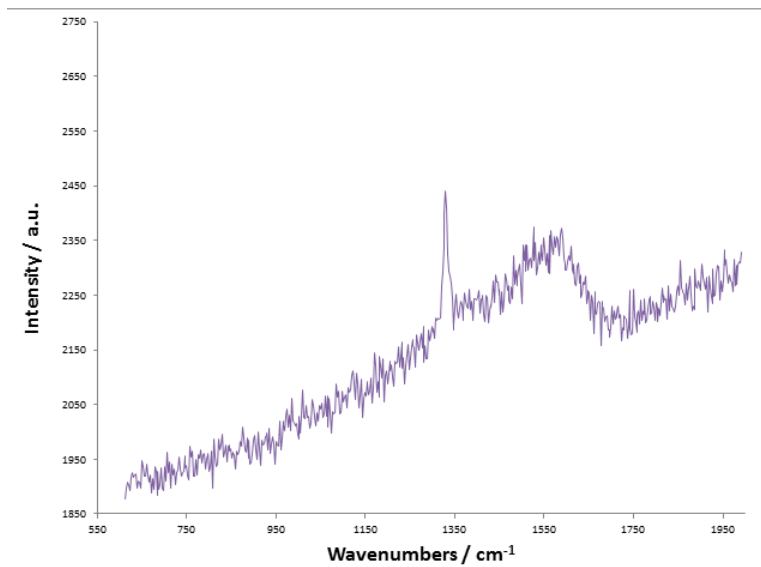


Figure 31. The visible Raman spectrum of boron doped diamond film etched in Ar/H<sub>2</sub> plasma.

Figure 31 shows the Raman spectrum of boron doped diamond film etched in an Ar/H<sub>2</sub> gas mixture. The similarity of this spectra to that of the undoped film etched under the same conditions (figure 27) suggests that the etching mechanism remains unaffected by the presence of boron in the film. However, in contrast to this, the Raman spectra for boron doped films etched with air and Ar/O<sub>2</sub> (figures 32 and 33 respectively) have an absence of the broad graphitic peak at 1580 cm<sup>-1</sup>, but an additional peak at 1120 cm<sup>-1</sup>. This signifies a possible difference in the processes involved during etching for these gas mixtures.

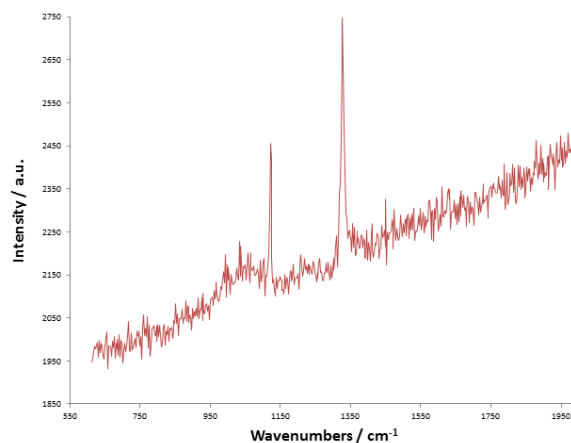


Figure 32. The visible Raman spectrum of boron doped diamond film etched in air plasma.

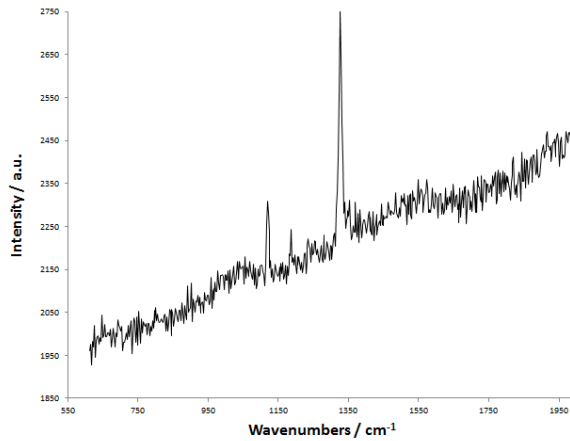


Figure 33. The visible Raman spectrum of boron doped diamond film etched in Ar/O<sub>2</sub> plasma.

The origin of the peak at 1120 cm<sup>-1</sup> remains to be undisputedly classified [45]. However it has been suggested that this peak is due to the presence of a form of sp<sup>2</sup> carbon [46]. The implication of this is that some alternative etching mechanism may be occurring in the cases where this peak is seen. However, without conclusive evidence for the origin of the peak, this is speculation only and in no way a reliable indication that an alternative mechanism is existent.

### 3.3.2 Formation Mechanism

The formation mechanism of diamond whiskers on boron doped diamond films is thought to differ considerably from that of undoped diamond. The position of diamond whiskers formed on boron doped films have been shown to correlate with the initial distribution of boron atoms within the film [42]. This is attributed to a higher concentration of electron emission from the boron sites [42,47], and it is this local electric field which initiates whisker formation in a similar way to that discussed for preferential formation at grain boundaries due to sp<sup>2</sup> inclusions. This is evidenced by the presence of diamond whiskers exclusively at grain boundaries when etching films in which the boron concentration is lowered to the extent that boron atoms only occupy inter-granular positions; progressive increase in the boron concentration causes boron atoms to extend increasingly farther away from the grain boundaries, and an equivalent whisker formation pattern is observed on etching [42].

The formation method proposed in section 1.5.4 above whereby whiskers originate from inherent surface roughness is rejected in the case of boron doped samples; the formation of diamond whiskers on smooth facets as described in reference [42] nulls this hypothesis, and is consistent with the boron impurities being the predominant factor in determining whisker location. However, the possibility of this mechanism contributing to whisker formation after surface etching at localised electric field sites has been initiated must not be disregarded.

### 3.3.3 Effect of Etching Gas

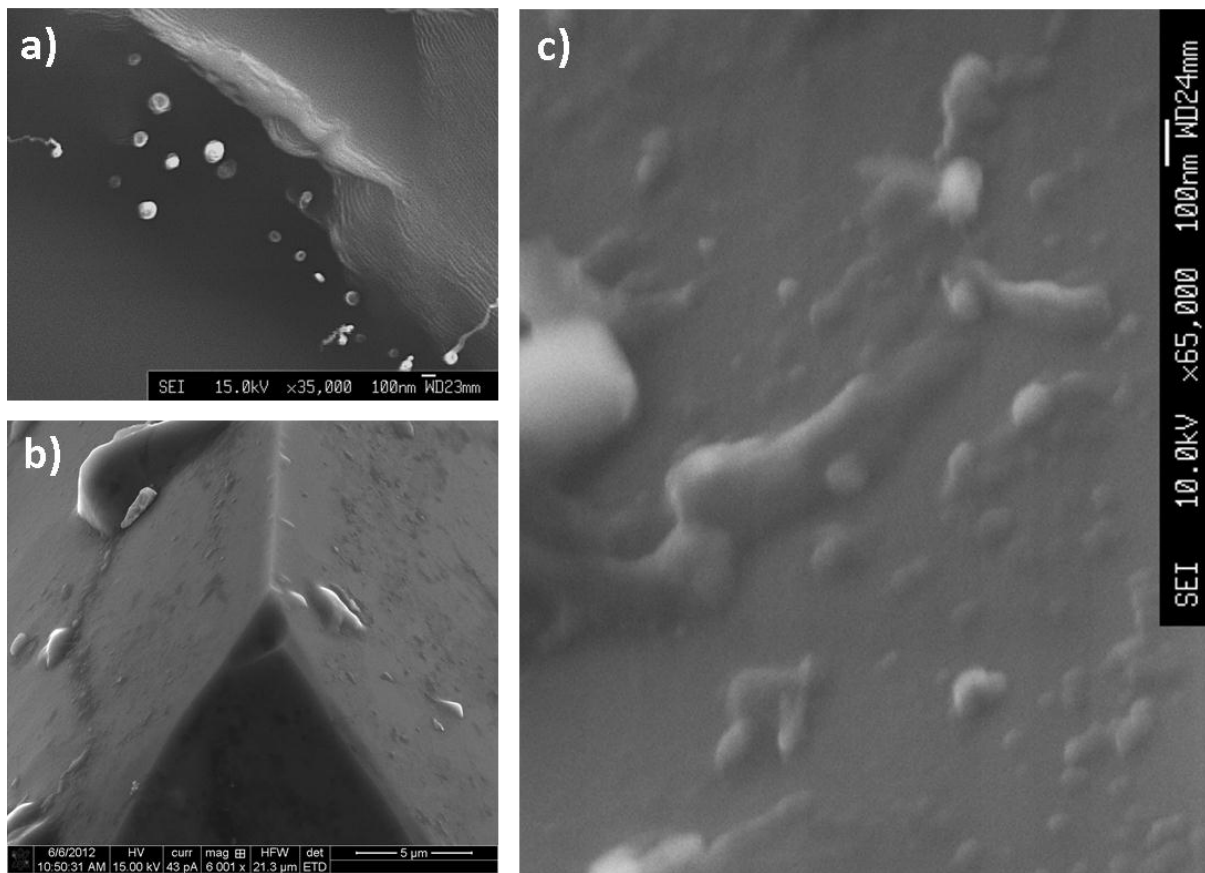


Figure 34. . FEGSEM micrographs of Ar/H<sub>2</sub> DC plasma etched boron doped diamond film; a) (20 min), top view b) (60 min), perspective tilt angle of 45° and c) (20 min), perspective tilt angle of 20°.

The images in figure 34 show the structures resulting from etching boron doped film with Ar/H<sub>2</sub> plasma. Again it is seen that some polishing effect has taken place, with a relatively smooth appearance to the nanostructures. As with the undoped samples, there is little evidence of diamond whisker formation, although figure 34 a does suggest that some early formation is present. The absence of whiskers following the second etch (figure 34 b) suggests that whisker formation is not limited by etch duration. Therefore, the absence of diamond whiskers is attributed to the low pressure used in etching; it has been reported that formation of dense, uniform diamond whiskers on boron doped diamond films requires gas pressures of the order 150 mtorr [42]. This requirement is believed to be due to the lower kinetic energy of ions in high density plasma, as discussed in section 3.2.1 above.

While the result is similar to that of undoped diamond films etched in the same gas mixture (figure 26), it appears that there may be a higher degree of anisotropic etching in the boron doped case. With the etching conditions being unchanged, this is attributed to the presence of boron in the sample; increased electron emission from boron sites is believed to cause localised etching [42], essentially focussing the etchant ions at specific points in an anisotropic manner.

Evidence of diamond whisker formation can clearly be seen for the air etched boron doped film (figure 35). The confinement of the whiskers to the grain boundaries is attributed to the higher concentration of sp<sup>2</sup> carbon in these areas, as outlined above. While the height of the whiskers is difficult to judge from a top view, it appears that the whiskers have developed more than in the Ar/H<sub>2</sub> case, and certainly are of higher density. This is expected due to the higher etch rate of oxygen

relative to a hydrogen based etching gas, and consistent with the findings of ref [42] for oxygen based etching at similar pressures.

Inspection of the surface after the second DC plasma etch found that there was no longer such a distinctive pattern of structures at grain boundaries. Figure 36 shows that some structures are still observed, but it would appear that these are different to those formed in the first etch. This may possibly be due to the longer etch duration meaning structures formed extend farther from the grain boundaries. The reason for the absence of the original structures however, is unknown, but suggests that they were of height less than the etch depth achieved on the second etch. This supports the theory that whisker formation in boron doped diamond films does not proceed via the mechanism proposed in reference [43], as discussed earlier (section 1.5.4), because the expectation of that mechanism here would be an amplification of the whiskers already formed.

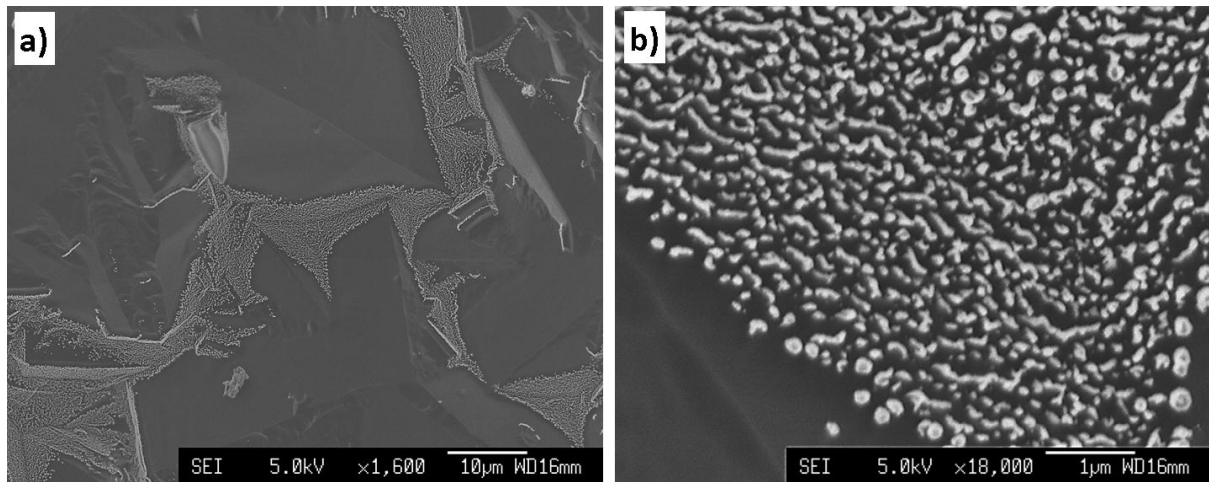


Figure 35. FEGSEM micrographs of air DC plasma etched (20 min) boron doped diamond film (top view).

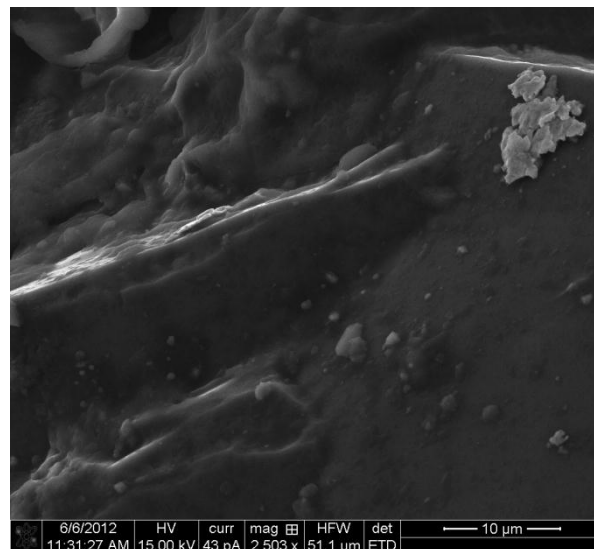


Figure 36. FEGSEM micrograph of air DC etched (60 min) boron doped diamond film.

The images in figure 37 show the surface morphology resulting from etching boron doped diamond film with Ar/O<sub>2</sub> plasma. This result is comparable to that of the Ar/H<sub>2</sub> etch (figure 34). A possible difference however is that the structures do not show quite the same level of whisker formation as those shown in figure 34 a. For the undoped diamond films it was suggested that the Ar/O<sub>2</sub> gas

mixture had a greater etching effect than the Ar/H<sub>2</sub> gas mixture, however for the boron doped film it appears that this is not the case. This is attributed to the differing etching mechanisms involved. It has been speculated that doping the diamond film with boron induces carbon defects in the diamond structure [42].

The result that Ar/H<sub>2</sub> has produced diamond structures which appear to be closer to forming diamond whiskers compared with the Ar/O<sub>2</sub> gas suggests that the chemical etching pathway plays a bigger part in the formation of diamond whiskers in boron doped films. This is intuitive, as the chemical pathway involves removal of non diamond carbon from the surface, which will be present in greater concentration in the boron doped samples due to defect influences.

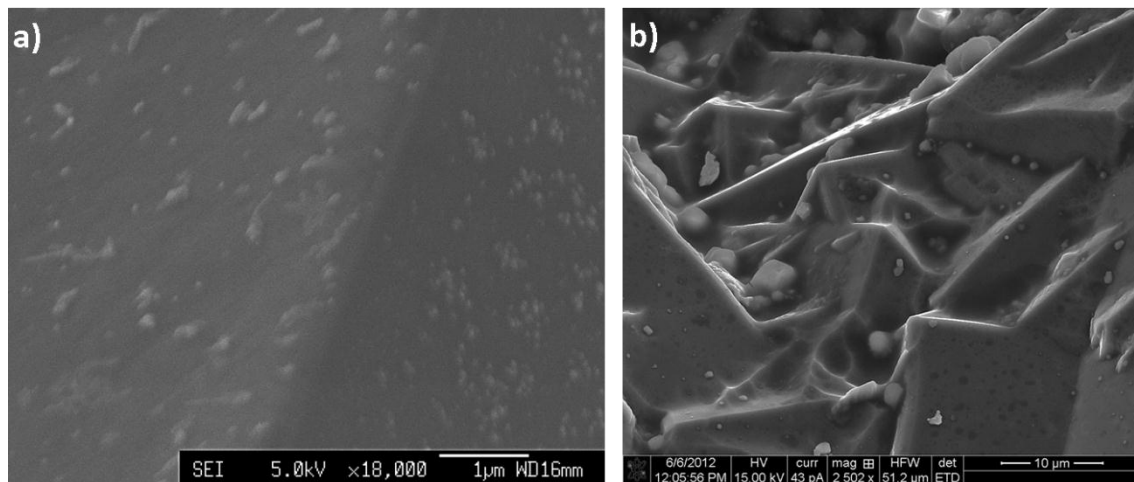


Figure 37. FEGSEM micrograph of Ar/O<sub>2</sub> DC plasma etched boron doped diamond film; a) 20 min, perspective tilt angle 20° and b) 60 min, perspective tilt angle 45°.

For all of the boron doped films, there has been evidence of surface nanostructure formation, although only weak evidence of the formation of diamond whiskers. It has been shown that the formation of diamond whiskers from boron doped diamond film, through a maskless plasma etching technique, is heavily dependent on the boron concentration [42]. The reported requirement of a boron concentration greater than  $8.4 \times 10^{20} \text{ cm}^{-3}$  for nanosized, densely packed whisker formation provides a possible explanation for the lack of whiskers observed in this research. While further experimentation would be required to determine if diamond whisker formation is possible under the given etching conditions, it is suggested that the concentration of boron within the films has limited formation of these structures.

While evidence of diamond whisker formation has been limited for all etching conditions in this research, the formation of surface structures as a result of etching has been observed in all cases. The implication of this is that while the techniques reported here certainly require refinement in order to allow production of uniform, reproducible diamond whiskers, they have shown that structure formation along with the potential for surface area increase are possible. Thus, diamond plasma etching may have significant applications in terms of hydrogen storage solutions.

## 4. Conclusion

Both boron doped and undoped CVD diamond films have been plasma etched with a variety of etching gas mixtures. The resultant surface morphology has been shown to be dependent on both the presence of boron in the film, and the etching gases used. The dependence of gas mixture has been attributed to the relative proportion of etching pathways undertaken in different gases.

Interpretation of the results has suggested that the formation mechanism of diamond whiskers in boron doped films is different from that in undoped films. Specifically, it is suggested that boron contributes to whisker formation through the following; the presence of boron increases the proportion of  $sp^2$  non-diamond carbon inclusions around the boron atoms, and this coupled with increased electron emission from boron sites, leads to localised etching.

Some inconsistencies with similar research reported in the literature have been observed, but justification for these has been given in terms of the different etching conditions used. Specifically, the absence of diamond whiskers in the etched films is thought to be due to the mild etching conditions used, along with the relatively low concentration of boron restricting whisker formation in the case of boron doped films. Significantly, the possibility of diamond whisker formation has been demonstrated, along with the necessity for specific reaction conditions in order to achieve this.

In order to further this investigation and obtain conclusive evidence to support the suggestions made in this report, additional experimental procedures are needed, as well as more extensive surface examination techniques. Varied etch durations, gas ratios, gas pressures and boron concentrations, as well as higher power etching techniques would all facilitate an enhanced understanding of the etching processes discussed in this report. An interesting area for further study would involve the quantitative characterisation of the surface, in terms of the positioning of  $sp^2$  carbon and boron atoms, prior to etching. This could then be used for direct comparison with the surface morphology after etching, providing insight into the mechanism of structure formation.

## 5. Acknowledgements

Thanks are due to Professor Paul May, Dr Neil Fox and Dr James Smith for scientific guidance and practical assistance throughout. Also to Dr Oliver Fox, Raquel Vaz and Liam Payne for their assistance in acquiring SEM images.

## 6. References

1. Z. Yuan, Z. Jin, R. Kang, Q. Wen, *Diamond Relat. Mater.* 21 (2012) 50
2. A.M. Zaitsev, G. Kosaca, B. Richarz, V. Raiko, R. Job, T. Fries, W.R. Fahrner, *Diamond Relat. Mater.*, 7 (1998) 1108
3. H. Tokura, C-F. Yang, M. Yoshikawa, *Thin Solid Films*, 212 (1992) 49
4. E. Paul, C.J. Evans, A. Mangameli, L. McGluaflin, R.S. Polvani, *Precision Engineering*, 18 (1996) 4
5. J. Haisma, F.J.H.M. van der Kruis, B.A.C.M. Spierings, J.M. Oomen, F.M.J.G. Fey, *Precision Engineering*, 14 (1992) 20
6. M. McCormack, S. Jin, J.E. Graebner, T.H. Tiefel, G.W. Kammlott, *Diamond Relat. Mater.*, 3 (1994) 254
7. S. Jin, J.E. Grabner, M. McCormack, T.H. Tiefel, A. Katz, W.C. Dautremont-Smith, *Letters to Nature*, 362 (1993) 822
8. I. Bello, M.K. Fung, W.J. Zhang, K.H. Lai, Y.M. Wang, Z.F. Zhou, R.K.W. Yu, C.S. Lee, S.T. Lee, *Thin Solid Films*, 368 (2000) 222
9. P.W. Leech, G.K. Reeves, A. Holland, *J. Mater. Science*, 36 (2001) 3453
10. G.S. Sandhu, W.K. Chu, *Appl. Phys. Lett.*, 55 (1989) 437
11. K. Kobayashi, N. Mutsukura, Y. Machi, *Thin Solid Films*, 200 (1991) 139
12. K. Kobayashi, K. Yamamoto, N. Mutsukura, Y. Machi, *Thin Solid Films*, 185 (1990) 71
13. C. Vivensang, L. Ferlazzo-Manin, M.F. Ravet, G. Turban, F. Rousseaux, A. Gicquel, *Diamond Relat. Mater.*, 5 (1996) 840
14. Y. Ando, Y. Nishibayashi, K. Kobashi, T. Hirao, K. Oura, *Diamond Relat. Mater.*, 11 (2002) 824
15. M. Yoshikawa, F. Okuzumi, *Surface and Coatings Technology*, 88 (1996) 254.
16. Q. Wang, J.J. Li, Z.L. Wang, C.Z. Gu, Z. Cui, *J. Phys. Chem. C* 111 (2007) 7058
17. N.N. Eframow, M.W. Geis, D.C. Flanders, G.A. Lincoln, N.P. Economou, *J. Vac. Sci. Technol. B*, 3 (1985) 416
18. S. Ilias, G. Sene, P. Muller, V. Stambouli, J. Pascallon, D. Bouchier, A. Gicquel, A. Tardieu, E. Anger, M.F. Ravert, *Diamond Relat. Mater.*, 5 (1996) 835
19. T.J. Whetten, A.A. Armstead, T.A. Gryzbowski, A.L. Ruoff, *J. Vac. Sci. Technol. A*, 2 (1984) 477
20. S. Preuss, M. Stuke, *Appl. Phys. Lett.* 67 (1995) 338
21. Q. Wu, Y. Ma, R. Fang, Y. Liao, Q. Yu, *Appl. Phys. Lett.* 82 (2003) 1703
22. S. Preuss, M. Spath, Y. Zhang, M. Stuke, *Appl. Phys. Lett.* 62 (1993) 3049
23. V.N. Tokarev, J.I.B. Wilson, M.G. Jubber, P. John, D.K. Milne, *Diamond Relat. Mater.* 4 (1995) 169
24. S. Gloor, S.M. Pimenov, E.D. Obraztsova, W. Luthy, H.P. Weber, *Diamond Relat. Mater.* 7 (1998) 607
25. G.A. Shafeev et.al. *J. Appl. Phys. A*, 65 (1997) 29
26. T.V. Kononenko, V.G. Ralchenko, I.I. Vlasov, S.V. Garnov, V.I. Konov, *Diamond Relat. Mater.*, 7 (1998) 1623
27. C.Y. Li, A. Hatta, *Diamond Relat. Mater.* 14 (2005) 1780
28. E.-S. Baik, Y.-J. Baik, S.W. Lee, D. Jeon, *Thin Solid Films* 377 (2000) 295
29. D.S. Hwang, T. Saito, N. Fujimori, *Diamond Relat. Mater.* 13 (2004) 2207
30. J.-Y. Lin, Z.-C. Li, C.-Y. Chen, L.-J. Chou, J.-C. Hwang, C.-S. Kou, *Diamond Relat. Mater.* 20 (2011) 922

31. W. McKenzie, J. Pethica, G. Cross, *Diamond Relat. Mater.*, 20 (2011) 707
32. O. Babchenko, A. Kromka, K. Hruska, M. Michalka, J. Potmesil, M. Vanecek, *Central European Journal of Physics*, 7 (2009) 310
33. W. Smirnov, J.J. Hees, D. Brink, W. Muller-Sebert, A. Kriele, O.A. Williams, C.E. Nebel, *Appl. Phys. Lett.*, 97 (2010) 073117
34. P.C. Yang, W. Liu, R. Schlessler, C.A. Wolden, R.F. Davis, J.T. Prater, Z. Sitar, *Journal Crystal Growth*, 187 (1998) 81
35. T. Ohashi, W. Sugimoto, Y. Takasu, *Diamond Relat. Mater.* 20 (2011) 1165
36. C.D. McGray, R.A. Allen, M. Cangemi, J. Geist, *Diamond Relat. Mater.*, 20 (2011) 1363
37. G.F. Ding, H.P. Mao, Y.L. Cai, Y.H. Zhang, X. Yao, X.L. Zhao, *Diamond and Relat. Mater.*, 14 (2005) 1534
38. P.P. Edwards, V.L. Kuznetsov, W.I.F. David, N.P. Brandon, *Energy Policy*, 36 (2008) 4356
39. M.A. Prelas, T.K. Ghosh, S.K. Loyalka, R.V. Tompson, *Journal Wide Bandgap Materials*, 10 (2002) 99
40. C.Y. Li, A. Hatta, *Diamond Relat. Mater.*, 15 (2006) 357
41. M.D. Stoikou, P. John, J.I.B. Wilson, *Diamond Relat. Mater.* 17 (2008) 1164
42. C. Terashima, K. Arihara, S. Okazaki, T. Shichi, D. A. Tryk, T. Shirafuji, N. Saito, O. Takai, A. Fujishima, *Applied Materials and Interfaces*, 3 (2011) 177
43. Q. Wang, C.Z. Gu, Z. Xu, J.J. Li, Z.L. Wang, *Journal Applied Physics*, 100 (2006) 034312
44. O. M. Kuttel, L. Diederich, E. Schaller, O. Carnal, L. Schlapbach, *Surface Science*, 337 (1995) L818
45. J. Birrell, J.E. Gerbi, O. Auciello, J.M. Gibson, J. Johnson, J.A. Carlisle, *Diamond Relat. Mater.*, 14 (2005) 86
46. A.C. Ferrari, J. Robertson, *Physical Review B*, 63 (2001) 121405(R)
47. A. Shih, J. Yater, P. Pehrsson, C. Hor, *Journal of Applied Physics*, 82 (1997) 1860